Nuclear Effects on Heavy Boson Production at RHIC and LHC

Xiaofei Zhang* and George Fai†

Center for Nuclear Research, Department of Physics, Kent State University

Kent, Ohio 44242, USA

February 5, 2002

Abstract

We predict $W^{\pm}$ and Z^0 transverse momentum distributions from proton-proton and nuclear collisions at RHIC and LHC. A resummation formalism with power corrections to the renormalization group equations is used. The dependence of the resummed QCD results on the non-perturbative input is very weak for the systems considered. Shadowing effects are discussed and found to be unimportant at RHIC, but important for LHC. We study the enhancement of power corrections due to multiple scattering in nuclear collisions and numerically illustrate the weak effects of the dependence on the nuclear mass.

PACS Numbers: 25.75.-q, 25.75.Dw, 24.85.+p, 14.70.-e, 12.38.Cy

*electronic mail: xiaofei@cnr4.physics.kent.edu

†electronic mail: fai@cnr4.physics.kent.edu

I. INTRODUCTION

With the commissioning of the Relativistic Heavy Ion Collider (RHIC), nuclear collision physics entered the collider era. New phenomena have been presented in $Au + Au$ collisions at the center-of-mass energy $\sqrt{s} = 130$ GeV/nucleon [1]. Negative hadron multiplicities are significantly increased compared to proton-antiproton collisions [2]. Some of the data, such as the antiproton-to-proton ratios [3], are reported to contradict perturbative Quantum Chromodynamics (pQCD) calculations. Initial efforts to understand hadron spectra from nuclear reactions at RHIC using pQCD have been published recently [4,5]. However, there is still a strong debate on how to apply pQCD to hadron production even in proton-proton (pp) collisions. With RHIC running at the full energy, and experiments at the Large Hadron Collider (LHC) at several TeV/nucleon soon to follow, "clean" processes, where pQCD works well in pp collisions, are needed to test pQCD in nuclear reactions at collider energies. It is particularly important to distinguish between expected nuclear effects and "new physics".

The production of $W^{\pm}$ and Z^0 bosons has been extensively studied at Tevatron energy ($\sqrt{s} = 1.8$ TeV). Perturbative QCD proved to be very successful in explaining the CDF [6] and D0 [7] data. Due to the large mass of $W^{\pm}$ and Z^0, and no final state rescattering in their production process, power corrections are expected to be small. Therefore, $W^{\pm}$ and Z^0 production could provide a bench mark test for pQCD at RHIC and LHC in both pp and nuclear collisions. Luminosity remains a concern at RHIC, in particular in pp collisions.

The bulk of the data for $W^{\pm}$ and Z^0 production is concentrated in the small transverse momentum (p_T) region, where p_T is much smaller than the corresponding heavy boson mass (M). When $p_T \ll M$, the p_T distributions calculated order-by-order in α_s in conventional fixed-order perturbation theory receive a large logarithm, $\ln(M^2/p_T^2)$, at every power of α_s, even in the leading order in α_s. Therefore, at sufficiently small p_T, the convergence of the conventional perturbative expansion in powers of α_s is impaired, and the logarithms must be resummed.

Resummation of the large logarithms in QCD can be carried out either in p_T-space

directly, or in the so-called "impact parameter", $\tilde{b}$-space, which is a Fourier conjugate of the p_T-space. (Since we are also interested in *nuclear* collisions, we reserve the notation b for the usual impact parameter associated with the geometry of colliding heavy nuclei, and denote the mathematical tool used in the resummation procedure by the symbol $\tilde{b}$.) Using the renormalization group equation technique, Collins and Soper improved the $\tilde{b}$-space resummation to resum all logarithms as singular as, $\ln^m(M^2/p_T^2)/p_T^2$, as $p_T \to 0$ [8]. In the frame work of this renormalization group improved $\tilde{b}$-space resummation, Collins, Soper, and Sterman (CSS) derived a formalism for the transverse momentum distribution of vector boson production in hadronic collisions [9]. In the CSS formalism, non-perturbative input is needed for the large $\tilde{b}$ region. The dependence of the pQCD results on the non-perturbative input is not weak if the original extrapolation proposed by CSS is used. Recently, a new extrapolation scheme was proposed, based on solving the renormalization group equations, including power corrections [10]. Using the new extrapolation formula, the dependence of the pQCD result on the non-perturbative input was significantly reduced. This was achieved without matching the fixed-order calculations. The results agree with the D0 nd CDF data very well in the entire p_T interval from $p_T \lesssim 1$ GeV to p_T as large as the the vector mass. In addition, in this new extrapolation formalism, power corrections can be studied systematically for pp to proton-nucleus (pA) to nucleus-nucleus (AB) collisions.

Factorization plays a key role in pQCD predictions of observables. At RHIC and LHC, nuclear collisions reach an unprecedented energy scale. Factorization can not be extrapolated easily to AB collisions from hadron-hadron collisions [11], and power corrections may become important [12]. There are two types of power corrections: (1) Power corrections directly to the physical observables (type-I) and (2) power corrections to the evolution of renormalization group equations (type-II). Type-I power correction are proportional to powers of (Λ_{QCD}/Q), Q being the physical large scale (momentum). These are small for $W^{\pm}$ and Z^0 production as a result of the large mass of the particles in question. Type-II power corrections are proportional to powers of (Λ_{QCD}/μ), with evolution scale μ. Therefore,

physical observables carry the effect of type-II power corrections for all $\mu[Q_0, Q]$, with the boundary condition at the scale Q_0. Even with large mass, $W^{\pm}$ and Z^0 can still carry a large effect of type-II power corrections. However, Ref. [10] provides a way to study the effect of type-II power corrections numerically. Based on the numerical results presented in Ref. [10], the effect of type-II power corrections is also expected to be small for heavy vector boson production in pp collisions. In nuclear collisions, type-II power corrections will be enhanced by the nuclear size. Here we study the effects of enhanced power correction in pA and AB collisions.

The rapidity distribution of $W^{\pm}$ and Z^0 bosons at LHC was calculated recently and the effect of shadowing was discussed in this context [13]. The decay spectrum of Z^0 was suggested as an alternative reference process for J/ψ suppression at LHC, since the Drell-Yan lepton pairs at low mass are expected to be dominated by $b\bar{b}$ decay. As most of the $W^{\pm}$ and Z^0 bosons observed in the experiment will be in the small transverse momentum region, it is of great interest to study the nuclear effects on massive gauge boson transverse momentum distributions. These effects include both the nuclear modification of the parton distribution function (shadowing), and the initial state power corrections. The second part of the present paper is devoted to these subjects.

The rest of the paper is organized as follows. In Section II, we review the CSS $\tilde{b}$-space resummation formalism and the new procedure [10] to extrapolate the pQCD calculation to the large $\tilde{b}$ region is outlined. We give predictions for $W^{\pm}$ and Z^0 transverse momentum distributions from pp collision at both RHIC and LHC energies. The sensitivity of the prediction to the non-perturbative parameters is discussed. Nuclear effects on $W^{\pm}$ and Z^0 transverse momentum distributions in pA and AB collisions are studied in Sections III and IV. In Section V, we present our conclusions. To make the paper reasonably self-contained, the Appendix summarizes relevant details of the CSS formalism. We use $\hbar = c = 1$ units.

II. TRANSVERSE MOMENTUM DISTRIBUTION OF HEAVY VECTOR BOSONS IN PROTON-PROTON COLLISIONS

In this Section, we briefly review the CSS $\tilde{b}$-space resummation formalism (Section II A). In Section II B we introduce the recently-proposed new formalism to extrapolate the perturbative calculation to the large $\tilde{b}$ region [10], and discuss the transverse momentum distribution of heavy vector bosons in pp collisions at RHIC and LHC energies.

A. Collins-Soper-Sterman (CSS) formalism

In the production of heavy vector bosons (of mass M), when $p_T \ll M$, the p_T distribution calculated order-by-order in α_s in conventional fixed-order perturbation theory receives a large logarithm, $\ln(M^2/p_T^2)$, at every power of α_s. Even at the leading order in α_s, the cross section $d\sigma/dM^2\,dy\,dp_T^2$ contains a term proportional to $(\alpha_s/p_T^2)\ln(M^2/p_T^2)$ coming from the partonic subprocess $q+\bar{q}\to V+g$, where $V=\gamma^*, W^\pm$ or Z^0. Beyond the leading order, we actually get two powers of the logarithm for every power of α_s, due to soft and collinear gluons emitted by the incoming partons. Therefore, at sufficiently small p_T, the convergence of the conventional perturbative expansion in powers of α_s is impaired, and the logarithms must be resummed.

For vector boson production in hadronic collisions between hadrons h_A and h_B, $h_A+h_B\to V(M)+X$ with $V=\gamma^*, W^\pm$, or Z^0, the CSS resummation formalism yields the following generic form [9]:

$$\frac{d\sigma(h_A+h_B\to V+X)}{dM^2\,dy\,dp_T^2}=\frac{1}{(2\pi)^2}\int d^2\tilde{b}\,e^{i\vec{p}_T\cdot\vec{\tilde{b}}}\,\tilde{W}(\tilde{b},M,x_A,x_B)+Y(p_T,M,x_A,x_B)\ , \qquad (1)$$

where $x_A=e^y\,M/\sqrt{s}$ and $x_B=e^{-y}\,M/\sqrt{s}$, with rapidity y and collision energy $\sqrt{s}$. In Eq. (1), the $\tilde{W}$ term dominates the p_T distributions when $p_T\ll M$, and the Y term gives corrections that are negligible for small p_T, but become important when $p_T\sim M$. In the CSS formalism, the function $\tilde{W}$ appears as a superposition,

$$\tilde{W}(\tilde{b}, M, x_A, x_B) = \sum_{ij} \tilde{W}_{ij}(\tilde{b}, M, x_A, x_B)\, \sigma_{ij\to V}(M) \ , \tag{2}$$

where $\sigma_{ij\to V}(M)$ is the lowest order cross section for a quark-antiquark pair of invariant mass M to annihilate into a vector boson V, and the $\sum_{ij}$ runs over all possible quark and antiquark flavors that can annihilate into the vector boson at the Born level [9]. In Eq. (2), $\tilde{W}_{ij}(\tilde{b}, M, x_A, x_B)$ is an effective flux to have partons of flavor i and j from the respective hadrons h_A and h_B, and it has the form

$$\tilde{W}_{ij}(\tilde{b}, M, x_A, x_B) = \mathrm{e}^{S(\tilde{b}, M)}\, \tilde{w}_{ij}(\tilde{b}, c/\tilde{b}, x_A, x_B) \ , \tag{3}$$

where $S(\tilde{b}, M)$ is given in the Appendix, and c is a constant of order unity [9,10]. The functions $\tilde{w}_{ij}(\tilde{b}, c/\tilde{b}, x_A, x_B)$ in Eq. (3) depend on only one momentum scale, $1/\tilde{b}$, and are perturbatively calculable as long as $1/\tilde{b}$ is large enough. All large logarithms from $\ln(1/\tilde{b}^2)$ to $\ln(M^2)$ in $\tilde{W}_{ij}(\tilde{b}, M, x_A, x_B)$ are completely resummed into the exponential factor $\exp[S(\tilde{b}, M)]$.

Since the perturbatively resummed $\tilde{W}_{ij}(\tilde{b}, M, x_A, x_B)$ in Eq. (3) is only reliable for the small $\tilde{b}$ region, an extrapolation to the large $\tilde{b}$ region is necessary in order to complete the Fourier transform in Eq. (1). This is the point where the dependence of the result on the nonperturbative parameters enters into the formalism, possibly limiting the predicative power of pQCD , especially for small p_T. We will next discuss this in detail.

B. Improved extrapolation formula with power corrections

The CSS formalism in its original form introduces a modification to the output of the perturbative calculation (see Appendix, Eq. (25)). The size of the modification depends on the non-perturbative input parameters, and can be as large as 50% of the perturbative result. Therefore the predictive power of the CSS formalism was questioned and new efforts have been devoted to resum the large logarithms directly in p_T space [14,15].

In oder to improve the predictive power of the CSS $\tilde{b}$-space resummation formalism, the following new form was proposed [10] by solving the renormalization group equation

including power corrections:

$$\tilde{W}(\tilde{b}, M, x_A, x_B) = \begin{cases} \tilde{W}(\tilde{b}, M, x_A, x_B) & \tilde{b} \leq \tilde{b}_{max} \\ \tilde{W}(\tilde{b}_{max}, M, x_A, x_B)\, F^{NP}(\tilde{b}, M, x_A, x_B; \tilde{b}_{max}, \alpha) & \tilde{b} > \tilde{b}_{max} \end{cases} , \quad (4)$$

where the nonperturbative function F^{NP} in Eq. (4) is given by

$$F^{NP}(\tilde{b}, M, x_A, x_B; \tilde{b}_{max}, \alpha) = \exp\left\{ -\ln\left(\frac{M^2 \tilde{b}_{max}^2}{c^2}\right)\left[g_1\left((\tilde{b}^2)^\alpha - (\tilde{b}_{max}^2)^\alpha\right) + g_2\left(\tilde{b}^2 - \tilde{b}_{max}^2\right)\right] - \bar{g}_2\left(\tilde{b}^2 - \tilde{b}_{max}^2\right)\right\} . \quad (5)$$

In Eq. (4) $\tilde{b}_{max}$ is a parameter to separate the perturbatively calculated part from the non-perturbative input. Unlike in the original CSS formalism, when $\tilde{b} \leq \tilde{b}_{max}$, the perturbatively calculated $\tilde{W}(\tilde{b}, M, x_A, x_B)$ is not altered and is independent of the nonperturbative parameters. In addition, the $\tilde{b}$-dependence in Eq. (5) is separated according to different physics origins. The $(\tilde{b}^2)^\alpha$-dependence mimics the summation of the perturbatively calculable leading power contributions to the kernels K and G in Eq.s (13) and (14) of the Appendix, respectively, to all orders in the running coupling constant $\alpha_s(\mu)$ with the scale μ running into the nonperturbative region [16]. The $\tilde{b}^2$-dependence of the g_2 term is a direct consequence of dynamical power corrections to the renormalization group equations of the kernels K and G, and has an explicit dependence on M. The $\bar{g}_2$ term represents the effect of the non-vanishing intrinsic parton transverse momentum. As we discuss later, these two terms behave differently in nuclear collisions.

A remarkable feature of the $\tilde{b}$-space resummation formalism is that the resummed exponential factor $\exp[S(\tilde{b}, M)]$ (see Eq. (3)) suppresses the $\tilde{b}$-integral when $\tilde{b}$ is larger than $1/M$. Therefore, when $M \gg \mu_0$, (where $\mu_0 \sim 1/\tilde{b}_{max}$ represents the scale at which pQCD starts to be applicable), it is possible that the Fourier transform in Eq. (1) is dominated by a region of $\tilde{b}$ much smaller than $1/\mu_0$, and the calculated p_T distributions are insensitive to the nonperturbative information at large $\tilde{b}$. In fact, it was shown using the saddle point method that, for a large enough M, a QCD perturbation calculation is valid even at $p_T = 0$ [17,9]. As discussed in Ref. [10], the value of the saddle point strongly depends

on the collision energy $\sqrt{s}$, in addition to its well-known M^2 dependence. Because of the steep evolution of parton distributions at small x, the $\sqrt{s}$ dependence of the $\tilde{W}$ in Eq. (1) significantly decreases the value of the saddle point and improves the predictive power of the $\tilde{b}$-space resummation formalism at collider energies.

To display the saddle point clearly, let us rewrite the first term on the right-hand side of Eq. (1), taking into account that there is no preferred transverse direction and that $\tilde{W}$ in Eq. (1) is a function of $\tilde{b} = |\vec{\tilde{b}}|$ only:

$$\frac{1}{(2\pi)^2} \int d^2\tilde{b}\, e^{i\vec{p}_T \cdot \vec{\tilde{b}}}\, \tilde{W}(\tilde{b}, M, x_A, x_B) = \frac{1}{2\pi} \int_0^\infty d\tilde{b}\, \tilde{b}\, J_0(p_T \tilde{b})\, \tilde{W}(\tilde{b}, M, x_A, x_B) \ , \tag{6}$$

where $\tilde{W}$ contains the exponential factor $\exp[S(\tilde{b}, M)]$, and $J_0(z)$ with $z = p_T\tilde{b}$ represents the Bessel function of order zero. When $p_T > 0$, the Bessel function suppresses the large $\tilde{b}$ region of the integration. Because the argument of the Bessel function is proportional to p_T, the large $\tilde{b}$ region is more suppressed if p_T is larger. In the following, we focus on the saddle point at $p_T = 0$. Fig. 1 is a graph (on an arbitrary scale) of the integrand of the right hand side of Eq. (6) with $p_T = 0$ for the case of Z^0 production at the collision energies where we intend to carry out our calculations: $\sqrt{s} = 350$ GeV (dotted line), $\sqrt{s} = 500$ GeV (short dashes), and at $\sqrt{s} = 5.5$ TeV (solid). The position of the saddle point decreases as the collision energy increases. We will show that the predictive power of the formalism is very good at RHIC. As a consequence of the behavior of the saddle point position, we expect excellent precision at $\sqrt{s} = 5.5$ TeV. At the LHC pp energy of $\sqrt{s} = 14$ TeV, the saddle point moves to even smaller values of $\tilde{b}$, improving the accuracy of the calculation even further.

The parameters g_1 and α of Eq. (5) are fixed by the requirement of continuity of the function $\tilde{W}(\tilde{b})$ and its derivative at $\tilde{b} = \tilde{b}_{max}$. (The results are insensitive to changes of $\tilde{b}_{max}$ in the interval 0.3 GeV$^{-1} \lesssim \tilde{b}_{max} \lesssim$ 0.7 GeV^{-1}. We use $\tilde{b}_{max} = 0.5$ GeV^{-1} in Ref. [10] and here.) The value of g_2 and $\bar{g}_2$ can be obtained by fitting the low-energy Drell-Yan data, and are taken to be $\bar{g}_2 \sim 0.27$ GeV^2, and $g_2 \sim 0.01$ GeV^2 following Ref.s [10] and [18]. As the $\tilde{b}$ dependence of the g_2 and $\bar{g}_2$ terms in Eq. (5) is identical, it is convenient to combine these

terms and define

$$G_2 = \ln(\frac{M^2 \tilde{b}_{max}^2}{c^2}) g_2 + \bar{g}_2 \ . \tag{7}$$

Using the values of the parameters listed above, we get $G_2 \sim 0.4$ GeV^2 for $W^\pm$ and Z^0 production in pp collisions. The parameter G_2 can be considered the only free parameter in the non-perturbative input in Eq. (5), arising from the power corrections in the renormalization group equation. Our results are not sensitive to small variations of G_2 around its estimated value. We use $G_2 = 0.4$ GeV^2 in the following. An impression about the importance of power corrections can be obtained by comparing results with $G_2 = 0.4$ GeV^2 to those with power corrections turned off ($G_2 = 0$). We therefore define the ratio of these quantities:

$$R_{G_2}(p_T) \equiv \frac{d\sigma^{(G_2)}(p_T)}{dp_T} \Big/ \frac{d\sigma(p_T)}{dp_T} \ . \tag{8}$$

The cross sections in the above equation and in the results presented in this paper have been integrated over rapidity and invariant mass squared from Eq. (1). For the integration over dM^2, we use the "narrow width approximation" [19]. With respect to rapidity, we integrate over the interval $[-1, 1]$ for RHIC, and over [-2.4,2.4] for LHC, representing the central acceptances of the appropriate detectors. For the parton distribution functions, we use the CTEQ5M set [20] in the present work.

The following figures display differential cross sections and the corresponding R_{G_2} ratios for Z^0 and $W^\pm$ production as functions of p_T, in order of increasing energy. (In what follows, by $W^\pm$ production cross section we mean the cross section for $W^+ + W^-$.) In Fig. 2(a) we show the differential cross section for Z^0 production in pp collisions at $\sqrt{s} = 500$ GeV, where a RHIC pp run is expected. The accompanying Fig. 2(b) displays R_{G_2} of Eq. (8). It can be seen that the R_{G_2} ratio converges to unity (i.e. very small power corrections) with increasing p_T, and the effect of power corrections is about five percent for $p_T = 0$. However, when $p_T > 2$ GeV, the deviation of R_{G_2} from unity is under two percent. A very similar conclusion can be drawn from Fig. 3, concerning $W^\pm$ production in pp collisions at the same energy: the dependence on the nonperturbative input is weak even at the lowest transverse momenta.

Fig.-s 4 and 5 contain similar information for Z^0 and $W^\pm$ production in pp collisions at the planned LHC nucleus-nucleus collision energy of $\sqrt{s} = 5.5$ TeV, while the cross section and R_{G_2} are given for the LHC pp energy of $\sqrt{s} = 14$ TeV in Fig.-s 6 and 7. At all energies, the magnitude of the $W^\pm$ production cross section is about 3 to 5 times that of the Z^0 production cross section. Otherwise, the results for Z^0 and $W^\pm$ production are very similar, because the saddle points are almost at the same place in $\tilde{b}$ space in the two cases. As it has been pointed out in Ref [10], the position of the saddle point is determined by two terms: the first term is inversely proportional to the mass of the vector boson, and the second term is proportional to the derivative of the parton distribution function with respect to the scale at x_A or x_B. At the collider energies considered here, the second term is negative. While M_W is a little smaller than M_Z, and thus the first term is larger for $W^\pm$ than for Z^0, the contribution from the second term will effect the saddle point for $W^\pm$ more than that of the Z^0 with a small x_A and x_B.

As expected from Fig. 1, the dependence on the nonperturbative input decreases with increasing collision energy. The R_{G_2} ratio is smaller than one percent at LHC for both $\sqrt{s} = 5.5$ TeV and $\sqrt{s} = 14$ TeV, even when $p_T = 0$. These results confirm that the predictive power of the formalism is very good at RHIC and excellent at LHC. They also show that the effect of power corrections is very small at LHC for almost the whole p_T region and it is also negligible for RHIC when p_T is larger than 2 GeV.

III. ISOSPIN AND SHADOWING EFFECTS IN NUCLEAR COLLISIONS

In lack of nuclear effects on the hard collision, the production of heavy vector bosons in nucleus-nucleus (AB) collisions should scale, compared to the production in pp collisions, as the number of hard collisions, AB. However, there are several nuclear effects on the hard collision in a heavy-ion reaction. We distinguish three categories of these effects: isospin effects, the modification of the parton distribution function in the nucleus, and the enhancement of power corrections by the nuclear size. In this Section we discuss the first

two of these nuclear effects. Power corrections will be treated separately in the next Section.

As the parton distribution of neutrons is different from that of the protons, the production cross section of heavy vector bosons in proton-neutron and neutron-neutron interactions differs from the corresponding production cross section in pp collisions. This difference is the source of the so-called isospin effects. To study the isospin effects, let us introduce

$$R_{iso}(p_T) \equiv \frac{d\sigma(p_T, Z_A/A, Z_B/B)}{dp_T} \Big/ \frac{d\sigma(p_T)}{dp_T} \ , \tag{9}$$

where Z_A and Z_B are the atomic numbers and A and B are the mass numbers of the colliding nuclei, and the cross section $d\sigma(p_T, Z_A/A, Z_B/B)/dp_T$ has been averaged over AB, while $d\sigma(p_T)/dp_T$ is the pp cross section (with $G_2 = 0$). Since the $u\bar{u}$ coupling in Z^0 production is replaced by $u\bar{d}$ coupling to produce $W^{\pm}$ bosons, we expect R_{iso} to be complementary for $W^{\pm}$ and Z^0 production, i.e. if one of these ratios is larger than one, the other ratio should be smaller than unity.

Next we turn to the phenomenon of shadowing. We use the term shadowing in the general sense, referring to all modifications of the parton distribution function in the environment of the nucleus [13]. This includes, in different regions of x, the phenomena of shadowing (in the strict sense), anti-shadowing, and the EMC effect. It is also important to note that we define shadowing effects as leading twist effects, not including power corrections [11]. Thus, shadowing effects and power correction are clearly separated in the present work.

In general, shadowing is expected to be a function of x, the scale Q, and of the position in the nucleus. The latter dependence means that in heavy-ion collisions, shadowing should be impact parameter (b) dependent. The parameterizations of shadowing in the literature take into account some of these effects, but no complete parameterization exists to date to our knowledge. For example, the HIJING parameterization includes impact parameter dependence, but does not deal with the scale dependence [21,22]. On the other hand, the EKS98 [23] and HKM [24] parameterizations have a scale dependence, but do not consider impact parameter dependence. (The latter parameterizations have been compared recently [25].) Since in this paper we concentrate on impact-parameter integrated results, where

the effect of the b-dependence of shadowing is relatively unimportant [5], and we focus more attention on scale dependence, we find the EKS98 shadowing parameterization most appropriate for our present purposes. Therefore we use EKS98 shadowing [23] in this work.

Similarly to Eq. (9) for isospin effects, we define a shadowing ratio,

$$R_{sh}(p_T) \equiv \frac{d\sigma^{(sh)}(p_T, Z_A/A, Z_B/B)}{dp_T} \Big/ \frac{d\sigma(p_T)}{dp_T} \ . \tag{10}$$

Thus, R_{sh} incorporates the effects of both shadowing and the isospin composition of the nuclei. Furthermore, in this Section we take $G_2 = 0$ throughout, switching off power corrections. The enhanced power corrections in pA and AB collisions will be discussed separately in the next Section.

Fig. 8 displays R_{iso} (dashed lines) and R_{sh} (full lines) as functions of p_T for Z^0 production (Fig. 8(a)) and $W^{\pm}$ production (Fig. 8(b)), respectively, at $\sqrt{s} = 350$ MeV. The same information is presented at $\sqrt{s} = 5.5$ TeV in Fig. 9. We find that $R_{iso} > 1$ for Z^0 production and $R_{iso} < 1$ for $W^{\pm}$ production at both energies, complementing each other, as expected. How close R_{iso} is to unity depends on the region of x that has the dominant contribution to the cross section. At LHC, $x \sim 0.02$, and the magnitude of the isospin effects is about 2%. This is because when x is in this range, the difference of the distributions of $u(\bar{u})$ and $d(\bar{d})$ quarks in the nucleus is very small. At RHIC, where the dominant $x \sim 0.26$, the isospin effects are about 20% in the small p_T region. We have also checked that the scale dependence of isospin effects is not important. In Fig. 8, we also show a dotted line, which is the ratio of R_{sh} to R_{iso}, and thus can be considered to display the effect of "pure shadowing". Pure shadowing appears as an approximately constant reduction of 3-5% at $x \sim 0.26$.

The appearance of R_{sh} (full lines) is more surprising at $\sqrt{s} = 5.5$ TeV (Fig. 9). Since at LHC, even at $p_T = 90$ GeV, $x \sim 0.05$, we are still in the "strict shadowing" region. Therefore, the fact that $R_{sh} > 1$ for 20 GeV $\lesssim p_T \lesssim$ 70 GeV is not "antishadowing"; rather, it is a consequence of the change of the shape of the cross section from pp to AB reactions. In pp collisions, the maximum of the cross section is at $p_T \approx 3.7$ GeV. In AB collisions, the peak is shifted by about 0.4 GeV in the direction of large transverse momenta. On the other

hand, the contributions from the scale $\mu \sim p_T$ to M have been resummed. Resummation plays a more important role for small p_T than for large p_T. In EKS98, the strict shadowing effect is more important for small scales, such as $p_T \sim 2-5$ GeV, than for $p_T \sim M$. Thus, a relatively small shift in the peak position brings about the rise of R_{sh} above unity. The shadowing ratio R_{sh} dips below one again at a certain p_T, to approach the fixed-order pQCD result when $p_T \sim M$. The situation in Fig. 9 can be understood by noting that shadowing in the resummed transverse momentum distributions is sensitive to the scale used to describe the nuclear effects on the parton distribution function.

After this discussion one may want to revisit Fig. 8 and ask why is R_{sh} flat at RHIC energies. The answer lies in the observation that the EMC region of x dominates the cross section at $\sqrt{s} = 350$ MeV. There is no sensitivity to the scale in that region in EKS98.

In summary, the shadowing effects in the p_T distribution of heavy bosons at RHIC and LHC are sensitive to the scale of the nuclear parton distribution. The available data on the scale dependence of nuclear parton distribution functions are very limited [23]. Theoretical studies (such as EKS98) are based on the the assumption that the nuclear parton distribution functions differ from the parton distributions in the free proton, but obey the same DGLAP evolution [23]. Therefore, the tranverse momentum distribution of heavy bosons at LHC in $Pb + Pb$ collisions can provide a further test of our understanding of the nuclear parton distributions.

IV. ENHANCED POWER CORRECTIONS IN NUCLEAR COLLISIONS

We have seen in Section II that the effect of power corrections on the resummed cross section is very weak in pp collisions at both RHIC and LHC. In pA and AB collisions, power corrections will be enhanced due to rescattering in the nucleus. In this Section we discuss the enhancement of power corrections in nuclear collisions.

As $\bar{g}_2$ represents the effect of the partons' non-vanishing intrinsic transverse momentum, it should not have a strong nuclear dependence. On the other hand, g_2 arises as a result of

dynamical power corrections, and should be enhanced by the nuclear size, i.e. proportional to $A^{1/3}$. Considering the enhancement, we get $G_2 \sim 0.8$ GeV^2 for $p+Au$ and $G_2 \sim 1.5$ GeV^2 for $Pb+Pb$ reactions.

In order to study the effects of power corrections, we now define $R_{G_2}^{sh}$ in nuclear collision as follows:

$$R_{G_2}^{sh}(p_T) \equiv \frac{d\sigma^{(G_2,sh)}(p_T, Z_A/A, Z_B/B)}{dp_T} \Big/ \frac{d\sigma^{(sh)}(p_T, Z_A/A, Z_B/B)}{dp_T} \ , \tag{11}$$

where the numerator represents the result of the full calculation, with isospin effects, shadowing, and power corrections taken into account, and the denominator was introduced in connection with Eq. (10) and contains no power corrections ($G_2 = 0$).

Fig.10(a) and Fig.11(a) present the $d\sigma^{(G_2,sh)}(p_T, Z_A/A, Z_B/B)$ for $W^{\pm}$ production at $\sqrt{s} = 350$ GeV in $p+Au$ reactions and $\sqrt{s} = 5.5$ TeV in $Pb+Pb$ collisions, respectively. In Fig. 10(b) the solid line is $R_{G_2}^{sh}$ in $p+Au$ collisions and the dashed line is R_{G_2} in pp collisions at the same energy. At $p_T \sim 0$ GeV, $R_{G_2}^{sh}$ is about 0.88, in contrast to about 0.95 in pp collisions. The effects of power corrections are enhanced about three times in $p+Au$ collision relative to pp collisions. However, even for $p_T \sim 0$, the effect of power corrections is only about 10%, and for $p_T > 2$ GeV, the effect remains under 5%. Thus the effect of power corrections is weak in $p+Au$ collisions at RHIC. As for the situation at LHC in $Pb+Pb$ collisions, displayed in Fig. 11, the effects of power corrections appear to be enhanced by a similar factor (about three) from pp to $Pb+Pb$ collisions at LHC. The reason for the similar enhancement is the interplay of the higher energy and the larger value of G_2 mentioned above. In any case, the enhanced power corrections remain under 3% in the [0,80] GeV p_T interval for $Pb+Pb$ at LHC. The results for Z^0 production are similar to those for $W^{\pm}$ production.

V. DISCUSSION AND CONCLUSION

We have demonstrated that the predictive power of a resummed pQCD calculation for heavy boson production is very good at RHIC and excellent at LHC, because the depen-

dence of the cross sections on the non-perturbative input is weak. This makes $W^{\pm}$ and Z^0 production reliably calculable at the energies considered. On the experimental side, $W^{\pm}$ and Z^0 production should be an early observable at LHC (with sufficiently high production rates) in both pp and nuclear collisions. At RHIC, production rates may remain on the low side, in particular in pp collisions. In all cases, the cross sections peak at relatively low transverse momenta, and we calculate the peak position for all systems considered.

We have examined the effects of the isospin composition of nuclei and of shadowing in nuclear collisions. We find that isospin effects are modest in $W^{\pm}$ and Z^0 production at the energies considered, while shadowing is relatively unimportant at RHIC, but plays an important role at LHC in shaping the transverse momentum distributions. This comes about because of the sensitivity of shadowing effects to the scale of the parton distribution functions. We also studied the magnitude of power corrections in pp and nuclear collisions. Power corrections are small in pp collisions, and, even though part of these corrections is enhanced in nuclear collisions by a factor of $A^{1/3}$, they remain below 10% (even at very low transverse momenta) in AB reactions.

As indicated by the above observations, the resummed pQCD formalism yields accurate results for $W^{\pm}$ and Z^0 transverse momentum distributions at RHIC and LHC. The production of heavy bosons can therefore serve as a further test of the nuclear parton distributions. In more general terms, $W^{\pm}$ and Z^0 production at RHIC and LHC provides a bench mark test of resummed pQCD for pp and nuclear collisions at these energies. We hope that our predictions will soon be compared to data.

ACKNOWLEDGMENTS

We thank T. Hallman, D. Keane, and R. Vogt for stimulating discussions and J.W. Qiu for a careful reading of the manuscript. This work was supported in part by the U.S. Department of Energy under Grant No. DE-FG02-86ER-40251 and by the NSF under Grant INT-0000211.

VI. APPENDIX

Here we summarize relevant details of the CSS formalism concerning the structure of the terms in Eq. (1). We address, in particular, the construction of the exponential factor $\exp[S(\tilde{b}, M)]$ in Eq. (3).

It was shown in Ref. [9] that for $\tilde{b} \ll 1/\Lambda_{\rm QCD}$, the function $\tilde{W}(\tilde{b}, M, x_A, x_B)$ of Eq. (1) is directly related to the singular parts of the p_T distribution as $p_T \to 0$. More precisely, $\tilde{W}(\tilde{b}, M, x_A, x_B)$ includes all singular terms like $\delta^2(\vec{p}_T)$ and $[\ln^m(p^2/p_T^2)/p_T^2]_{\rm reg}$ with $m \geq 0$. Less singular terms as $p_T \to 0$ are included in the Y term of Eq. (1). The QCD resummation of the large logarithms in the CSS formalism is achieved by solving the evolution equation for the $\tilde{W}_{ij}$ of Eq. (2),

$$\frac{\partial}{\partial \ln M^2}\tilde{W}_{ij}(\tilde{b}, M, x_A, x_B) = \Big[K(\tilde{b}\mu, \alpha_s(\mu)) + G(M/\mu, \alpha_s(\mu))\Big]\, \tilde{W}_{ij}(\tilde{b}, M, x_A, x_B) \ , \qquad (12)$$

and the corresponding renormalization group equations for the kernels K and G,

$$\frac{\partial}{\partial \ln \mu^2}K(\tilde{b}\mu, \alpha_s(\mu)) = -\frac{1}{2}\gamma_K(\alpha_s(\mu)) \ , \qquad (13)$$

$$\frac{\partial}{\partial \ln \mu^2}G(M/\mu, \alpha_s(\mu)) = \frac{1}{2}\gamma_K(\alpha_s(\mu)) \ . \qquad (14)$$

The anomalous dimension $\gamma_K(\alpha_s(\mu)) = \sum_{n=1} \gamma_K^{(n)}(\alpha_s(\mu)/\pi)^n$ in Eqs. (13) and (14) is perturbatively calculable [9]. The renormalization group equations (13) and (14) for K and G ensure the correct renormalization scale dependence,

$$\frac{d}{d \ln \mu^2}\tilde{W}(\tilde{b}, M, x_A, x_B) = 0 \ . \qquad (15)$$

The solution given in Eq. (3) corresponds to simultaneously solving the evolution equation (12) from $\ln(c^2/\tilde{b}^2)$ to $\ln(M^2)$, and the renormalization group equations (13) and (14) from $\ln(c^2/\tilde{b}^2)$ to $\ln(\mu^2)$ and from $\ln(M^2)$ to $\ln(\mu^2)$, respectively, where c is a constant of order unity.

Integrating Eq. (13) from $\ln(c^2/\tilde{b}^2)$ to $\ln(\mu^2)$, and Eq. (14) from $\ln(M^2)$ to $\ln(\mu^2)$, one derives

$$K(\tilde{b}\mu, \alpha_s(\mu)) + G(M/\mu, \alpha_s(\mu)) = -\int_{c^2/\tilde{b}^2}^{M^2} \frac{d\bar{\mu}^2}{\bar{\mu}^2} A(\alpha_s(\bar{\mu})) - B(\alpha_s(M)) \ , \tag{16}$$

where A is a function of $\gamma_K(\alpha_s(\bar{\mu}))$ and $K(c, \alpha_s(\bar{\mu}))$ while B depends on both $K(c, \alpha_s(M))$ and $G(1, \alpha_s(M))$. The functions A and B do not have large logarithms and have perturbative expansions $A = \sum_{n=1} A^{(n)}(\alpha_s/\pi)^n$ and $B = \sum_{n=1} B^{(n)}(\alpha_s/\pi)^n$, respectively. The first two coefficients in the perturbative expansions are known [9,26]:

$$\begin{aligned}
A^{(1)} &= C_F \ , \\
A^{(2)} &= \frac{C_F}{2}\left[N\left(\frac{67}{18} - \frac{\pi^2}{6}\right) - \frac{10}{9} T_R\, n_f\right] , \\
B^{(1)} &= -\frac{3}{2} C_F \, , \\
B^{(2)} &= \left(\frac{C_F}{2}\right)^2 \left[\pi^2 - \frac{3}{4} - 12\zeta(3)\right] + \frac{C_F}{2} N \left[\frac{11}{18}\pi^2 - \frac{193}{24} + 3\zeta(3)\right] \\
&\quad + \frac{C_F}{2} T_R\, n_f \left[\frac{17}{6} - \frac{2}{9}\pi^2\right] ,
\end{aligned} \tag{17}$$

where $N = 3$ for SU(3) color, the color factor $C_F = (N^2-1)/2N = 4/3$ for quarks, $T_R = 1/2$, and n_F is the number of active quark flavors. The coefficients A and B given in Eq. (17) are derived from the general expressions in Ref. [9] with renormalization constant $c = 2\mathrm{e}^{-\gamma_E}$, where $\gamma_E \approx 0.577$ is Euler's constant [8].

Substituting Eq. (16) into Eq. (12), and integrating from $\ln(c^2/\tilde{b}^2)$ to $\ln(M^2)$, one obtains the $\tilde{W}_{ij}$ given in Eq. (3) with

$$S(\tilde{b}, M) = -\int_{c^2/\tilde{b}^2}^{M^2} \frac{d\bar{\mu}^2}{\bar{\mu}^2} \left[\ln\left(\frac{M^2}{\bar{\mu}^2}\right) A(\alpha_s(\bar{\mu})) + B(\alpha_s(\bar{\mu}))\right] . \tag{18}$$

In Eq. (3), all large logarithms from $\ln(c^2/\tilde{b}^2)$ to $\ln(M^2)$ in $\tilde{W}_{ij}(\tilde{b}, M, x_A, x_B)$ are completely resummed into the exponential factor $\exp[S(\tilde{b}, M)]$, leaving the $\tilde{w}_{ij}(\tilde{b}, c/\tilde{b}, x_A, x_B)$ with only one momentum scale $1/\tilde{b}$. The $\tilde{w}_{ij}(\tilde{b}, c/\tilde{b}, x_A, x_B)$ in Eq. (3) is then perturbatively calculable when the momentum scale $1/\tilde{b}$ is large enough, and is given by [9,14]

$$\tilde{w}_{ij}(\tilde{b}, c/\tilde{b}, x_A, x_B) = f_{i/A}(x_A, \mu = c/\tilde{b})\, f_{j/B}(x_B, \mu = c/\tilde{b}) \, . \tag{19}$$

The functions $f_{i/A}$ and $f_{j/B}$ are the modified parton distributions [9,14],

$$f_{i/A}(x_A,\mu) = \sum_a \int_{x_A}^1 \frac{d\xi}{\xi}\, C_{i/a}(x_A/\xi,\mu))\, \phi_{a/A}(\xi,\mu) \ , \tag{20}$$

where $\sum_a$ runs over all parton flavors. In Eq. (20), $\phi_{a/A}(\xi,\mu)$ is the normal parton distribution for finding a parton of flavor a in hadron A, and $C_{i/a} = \sum_{n=0} C_{i/a}^{(n)}(\alpha_s/\pi)^n$ are perturbatively calculable coefficient functions for finding a parton i in the modified parton distribution $f_{i/A}(x_A,\mu)$ from a parton a in the normal parton distribution $\phi_{a/A}(\xi,\mu)$. The first two coefficients of the $C_{i/a}$ are available [9,26]:

$$\begin{aligned}
&C_{i/j}^{(0)}(z,\mu = c/\tilde{b}) = \delta_{ij}\,\delta(z-1)\,,\\
&C_{i/g}^{(0)}(z,\mu = c/\tilde{b}) = 0\,,\\
&C_{i/j}^{(1)}(z,\mu = c/\tilde{b}) = \delta_{ij}\frac{C_F}{2}\left[(1-z) + \left(\frac{\pi^2}{2} - 4\right)\delta(1-z)\right],\\
&C_{i/g}^{(1)}(z,\mu = c/\tilde{b}) = T_R\, z\,(1-z) \ ,
\end{aligned} \tag{21}$$

where i and j represent quark or antiquark flavors and g represents a gluon. The coefficient functions given in Eq. (21) are derived from the general functional forms in Ref. [9] by setting the renormalization constants and the factorization scale as, $C_1 = c$, $C_2 = 1$, and $\mu = c/\tilde{b}$.

The $\sigma_{ij\to V}(M)$ in Eq. (2) is the lowest order cross section for a quark-antiquark pair to annihilate into the vector boson ($V = \gamma^*$, $W^\pm$, or Z^0). For $V = Z^0$, we have [8]

$$\sigma_{ij\to Z^0}(M_Z) = Q_{ij}\left(\frac{4\pi^3\alpha_{EM}^2(M_z)}{3s}\right) \ , \tag{22}$$

where Q_{ij} is the weak charge,

$$Q_{ij} = \frac{[1 - 4|e_q|\sin^2\theta_W]^2 + 1}{16\sin^2\theta_W\cos^2\theta_W} \ , \tag{23}$$

with θ_W denoting the Weinberg angle and e_q denoting the charge of the quark. Here, i and j must represent a quark-antiquark pair of the same flavor. For the Weinberg angle we use $\sin^2\theta_W = 0.23$. The $\sigma_{ij\to V}(M)$ for $V = W^\pm$ and γ^* can be found in Refs. [9,14].

In the CSS resummation formalism, the Y term in Eq. (1) represents a small correction to the p_T distribution when $p_T \ll M$. However, the Y term dominates the p_T-distributions when $p_T \sim M$. The Y term has the perturbative expansion $Y = \sum_{n=1} Y^{(n)}(\alpha_s(\mu)/\pi)^n$, and the coefficients $Y^{(n)}$ have the factorized form [9]

$$Y^{(n)}(p_T, M, x_A, x_B; \mu) = \sum_{a,b} \int_{x_A}^1 \frac{d\xi_A}{\xi_A}\, \phi_{a/A}(\xi_A, \mu) \int_{x_B}^1 \frac{d\xi_B}{\xi_B}\, \phi_{b/B}(\xi_B, \mu)$$
$$\times \left(\frac{4\pi^3 \alpha^2_{EM}(M_z)}{3s} \right) \; R^{(n)}_{ab\to V}(p_T, M, x_A/\xi_A, x_B/\xi_B; \mu) \;\; , \qquad (24)$$

where $\sum_{a,b}$ runs over all possible parton flavors and μ represents both the factorization and renormalization scales. The $R^{(n)}_{ab\to V}$ in Eq. (24) are perturbatively calculable and have the same normalization as those introduced in Ref. [9].

Since the perturbatively resummed $\tilde{W}_{ij}(\tilde{b}, M, x_A, x_B)$ in Eq. (3) is only reliable for the small $\tilde{b}$ region, an extrapolation to the large $\tilde{b}$ region is necessary in order to complete the Fourier transform in Eq. (1). In the original CSS formalism, a variable $\tilde{b}_*$ and a nonperturbative function $F^{NP}_{CSS}(\tilde{b}, M, x_A, x_B)$ were introduced [9] in such a way that $\tilde{W}$ was modified for all $\tilde{b}$ (except $\tilde{b} = 0$) as

$$\tilde{W}^{\rm CSS}(\tilde{b}, M, x_A, x_B) \equiv \tilde{W}(\tilde{b}_*, M, x_A, x_B)\, F^{NP}_{CSS}(\tilde{b}, M, x_A, x_B)\,, \qquad (25)$$

where $\tilde{b}_* = \tilde{b}/\sqrt{1 + (\tilde{b}/\tilde{b}_{max})^2}$, with $\tilde{b}_{max} = 0.5$ GeV^{-1}. This construction ensures that $\tilde{b}_* \leq \tilde{b}_{max}$ for all values of $\tilde{b}$. The function F^{NP}_{CSS} is a Gaussian in $\tilde{b}$, $F^{NP}_{CSS} \sim \exp(-\kappa \tilde{b}^2)$ with κ having a certain M^2, x_A, and x_B dependence [9].

As it has been pointed out in this paper and earlier [10], the original CSS extrapolation introduces a modification to the perturbative calculation, and the size of the modifications depends on the non-perturbative parameters in $F^{NP}_{CSS}(\tilde{b}, M, x_A, x_B)$. This motivated the development of the alternative extrapolation formula [10] used in the present work.

REFERENCES

[1] Proceedings of *Quark Matter 2001*, Nucl. Phys. A **698**, 1 (2002); http://www.rhic.bnl.gov/qm2001.

[2] C. Adler *et al.* (STAR) Phys. Rev. Lett. **87** 112303 (2001).

[3] G. David *et al.* (PHENIX), Nucl. Phys. A **698**, 227 (2002), nucl-ex/0105014; K. Adcox *et al.* (PHENIX), nucl-ex/0109003.

[4] E. Wang and X-N. Wang, Phys. Rev. Lett. **87**, 142301 (2001).

[5] Y. Zhang, G. Fai, G. Papp, G.G. Barnafoldi, and P. Levai, Phys. Rev. C **65**, 0349XX (2002).

[6] T. Affolder *et al.*, CDF Collaboration, Phys. Rev. Lett. **84**, 845 (2000).

[7] B. Abbott *et al.*, D0 Collaboration, hep-ex/0010026.

[8] J.C. Collins and D.E. Soper, Nucl. Phys. B **193**, 381 (1981); Erratum **213**, 545 (1983); **197**, 446 (1982).

[9] J.C. Collins, D.E. Soper and G. Sterman, Nucl. Phys. B **250**, 199 (1985).

[10] J. Qiu and X. Zhang, Phys. Rev. Lett. **86**, 2724 (2001); Phys. Rev. D **63**, 114011 (2001).

[11] J. Qiu and G. Sterman,hep-ph/0111002, to appear in the Proceedings of the Hard Probe Collaboration.

[12] J. Qiu and X. Zhang, hep-ph/0109210, to be appear in Phys. Lett. **B**.

[13] R. Vogt, Phys. Rev. **C64** 044901(2001).

[14] R.K. Ellis, D.A. Ross and S. Veseli, Nucl. Phys. **B503** 309 (1997).

[15] R.K. Ellis and S. Veseli, Nucl. Phys. **B511** 649 (1998).

[16] D. Appell, G. Sterman, and P. Mackenzie, Nucl.Phys. **B309**, 259 (1988).

[17] G. Parisi and R. Petronzio, Nucl. Phys. **B154**, 427 (1979).

[18] X. Zhang and G. Fai, in preparation.

[19] R. K. Ellis, W. J. Stirling, and B. R. Webber, *QCD and Collider Physics*, Cambridge, England, 1996.

[20] H. L. Lai et al., Eur. Phys. J. C **12**, 375(2000).

[21] X.N. Wang and M. Gyulassy, Phys. Rev. D **44**, 3501 (1991).

[22] S. Li and X.N. Wang, nucl-th/0110075.

[23] K.J. Eskola, V.J. Kolhinen, and C.A. Salgado, Eur. Phys. J. C **9**, 61 (1999).

[24] M. Hirai, S. Kumano, and M. Miyama, Phys. Rev. D **64**, 034003 (2001).

[25] K.J. Eskola, H. Honkanen, V.J. Kolhinen, and C.A. Salgado, hep-ph/0201256 (2002).

[26] C.T. Davies, B.R. Webber and W.J. Stirling, Nucl. Phys. **B256**, 413 (1985).

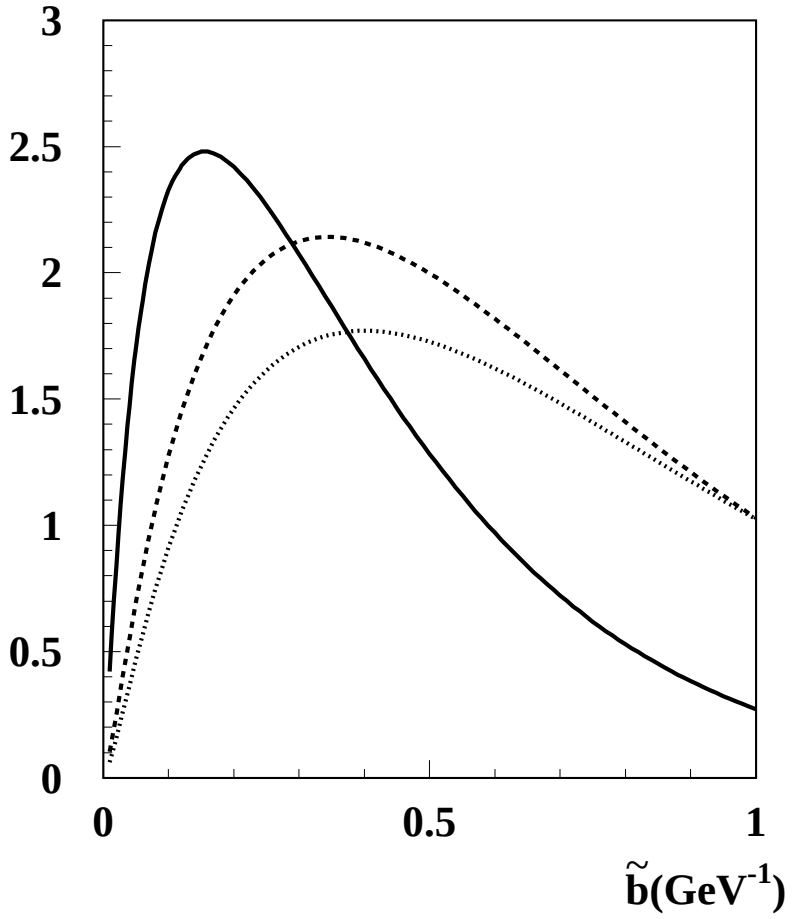

FIG. 1. Integrand of the $\tilde{b}$-integration in Eq. (6) at $p_T = 0$ for Z^0 as a function of $\tilde{b}$ with an arbitrary normalization at $\sqrt{s} = 350$ GeV (dotted line), $\sqrt{s} = 500$ GeV (dashed), and $\sqrt{s} = 5.5$ TeV (solid).

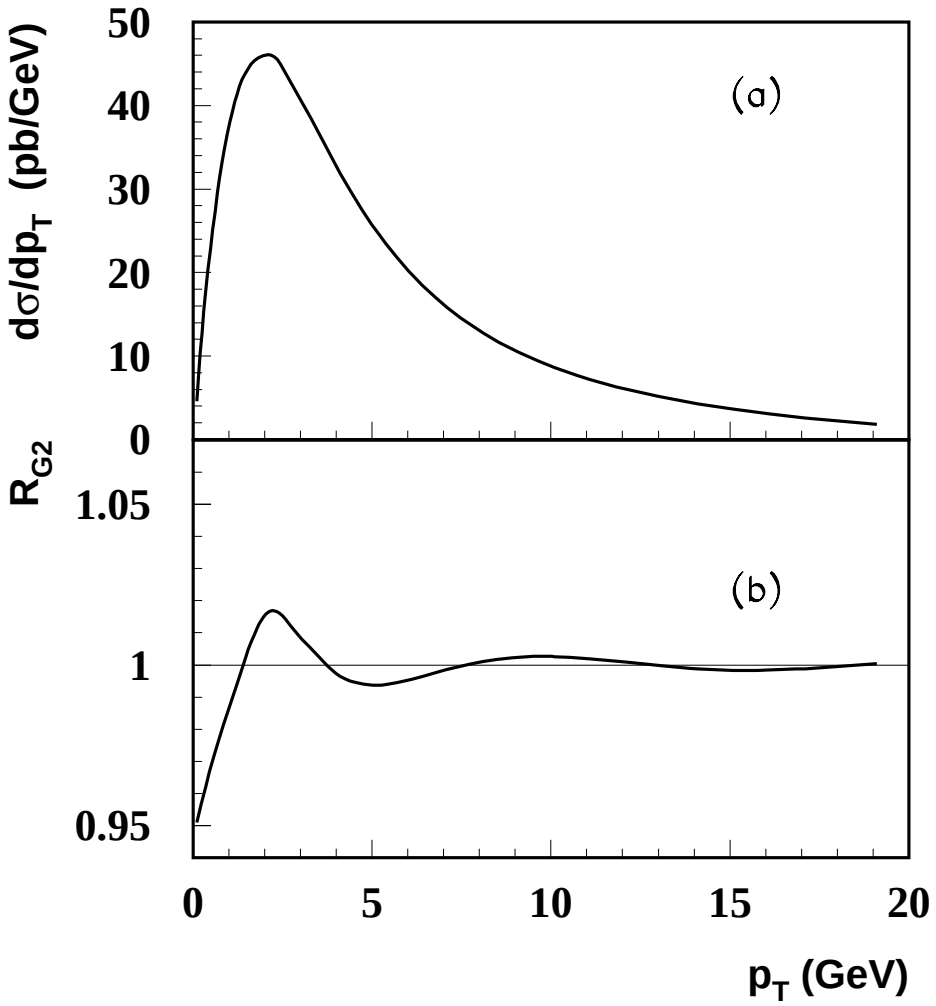

FIG. 2. (a) Cross section $\frac{d\sigma}{dp_T}$ for Z^0 production in pp collisions at RHIC with $\sqrt{s} = 500$ GeV; (b) R_{G_2} defined in Eq. (8) for Z^0 at the same energy.

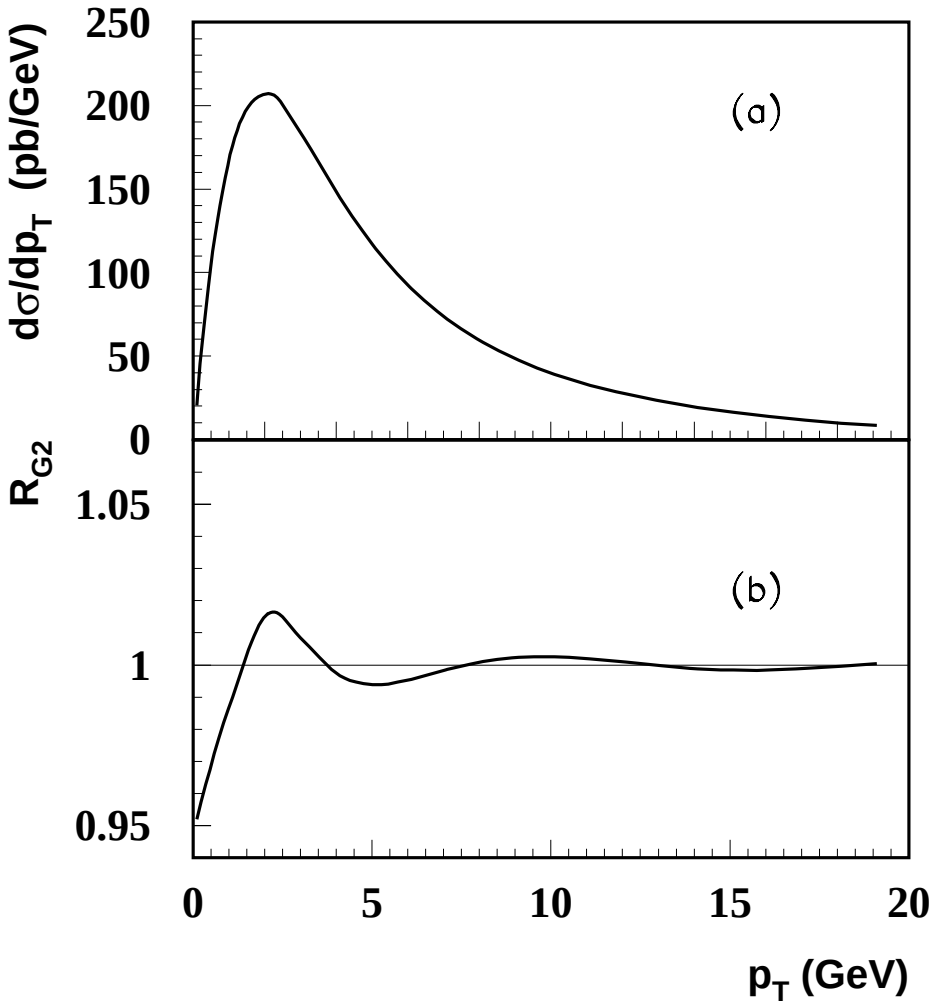

FIG. 3. (a) Cross section $\frac{d\sigma}{dp_T}$ for $W^{\pm}$ production in pp collisions at RHIC with $\sqrt{s} = 500$ GeV; (b) R_{G_2} defined in Eq. (8) for $W^{\pm}$ at the same energy.

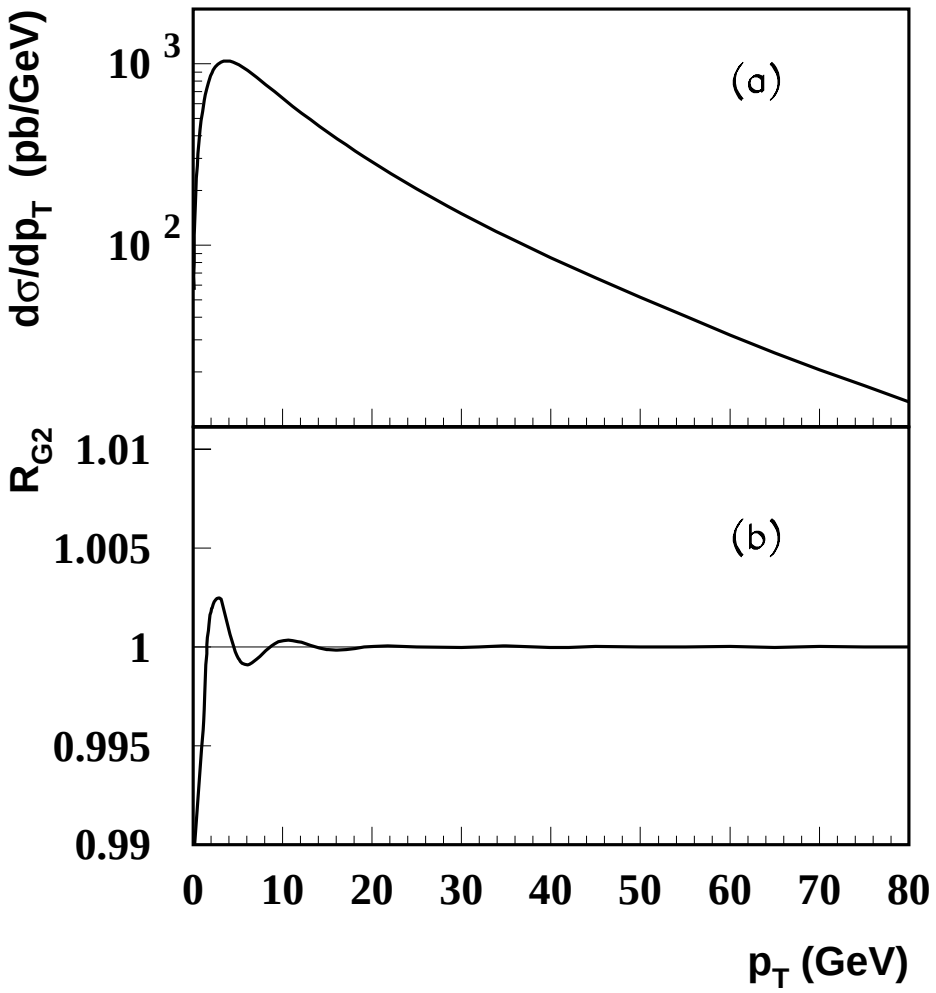

FIG. 4. (a) Cross section $\frac{d\sigma}{dp_T}$ for Z^0 production in pp collisions at LHC with $\sqrt{s} = 5.5$ TeV; (b) R_{G_2} defined in Eq. (8) for Z^0 at the same energy.

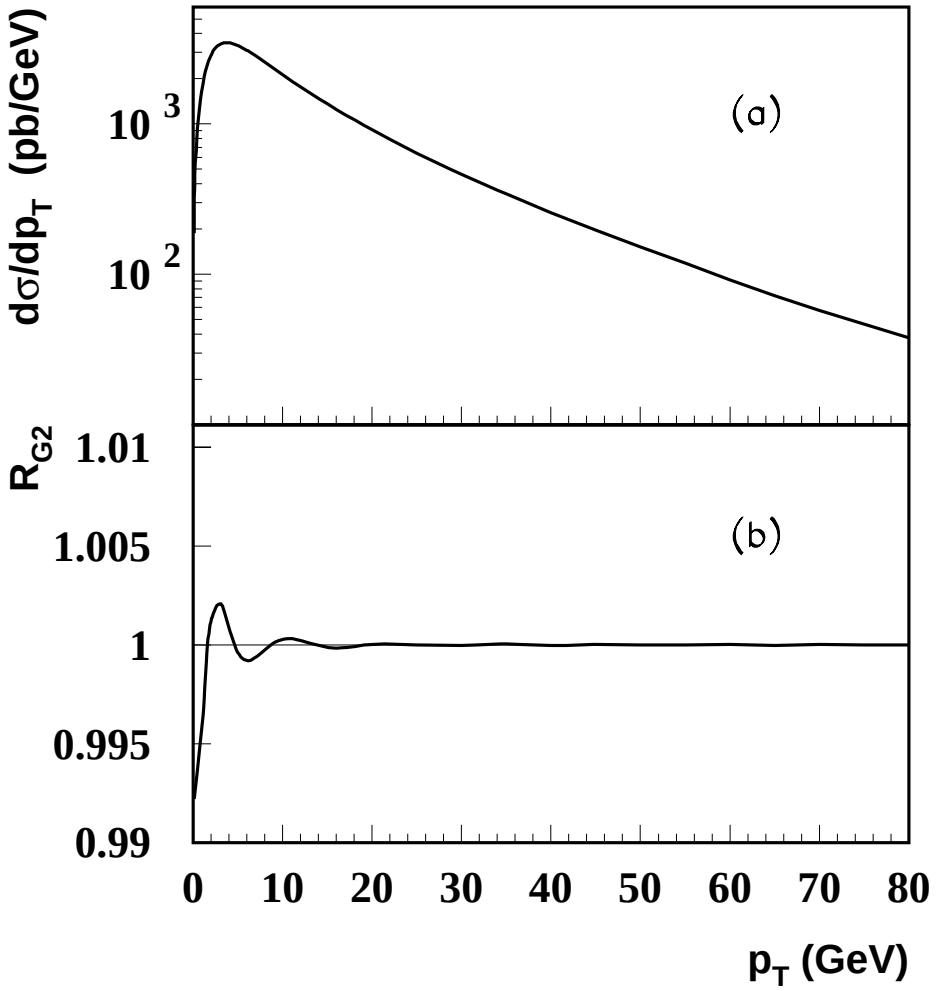

FIG. 5. (a) Cross section $\frac{d\sigma}{dp_T}$ for $W^{\pm}$ production in pp collisions at LHC with $\sqrt{s} = 5.5$ TeV; (b) R_{G_2} defined in Eq. (8) for $W^{\pm}$ at the same energy.

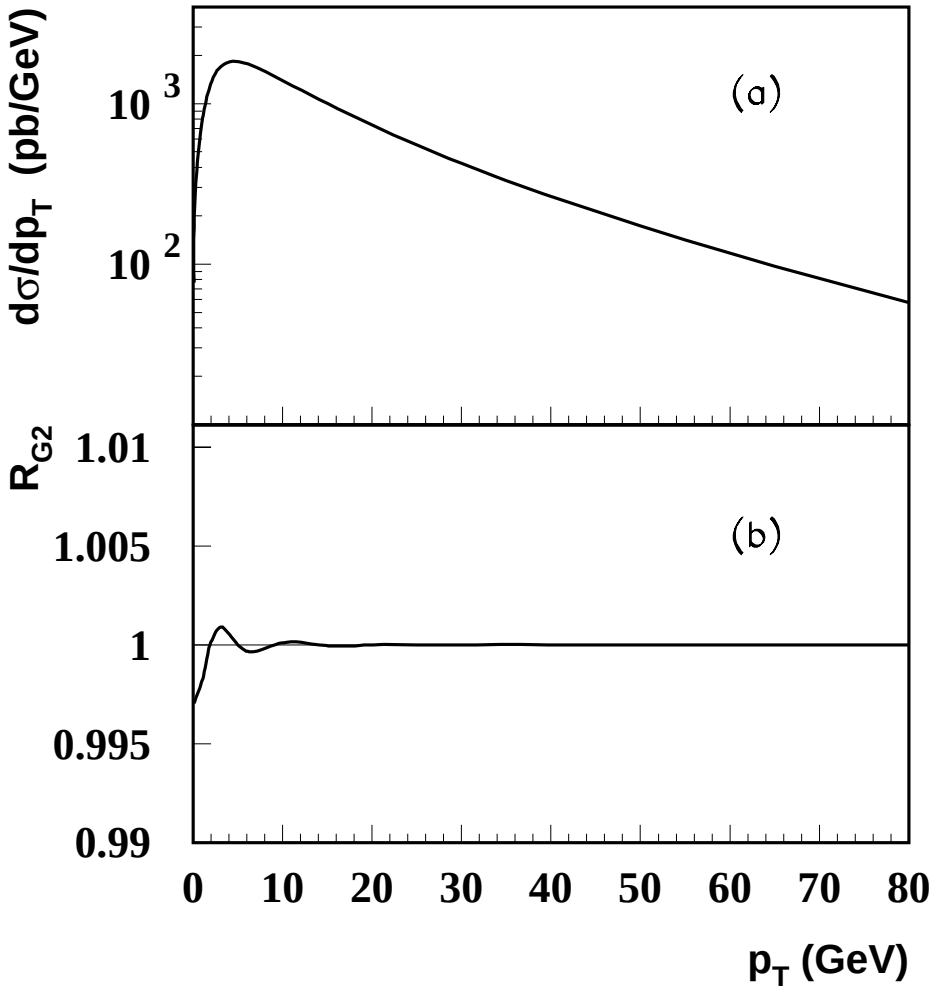

FIG. 6. (a) Cross section $\frac{d\sigma}{dp_T}$ for Z^0 production in pp collisions at LHC with $\sqrt{s} = 14$ TeV; (b) R_{G_2} defined in Eq. (8) for Z^0 at the same energy.

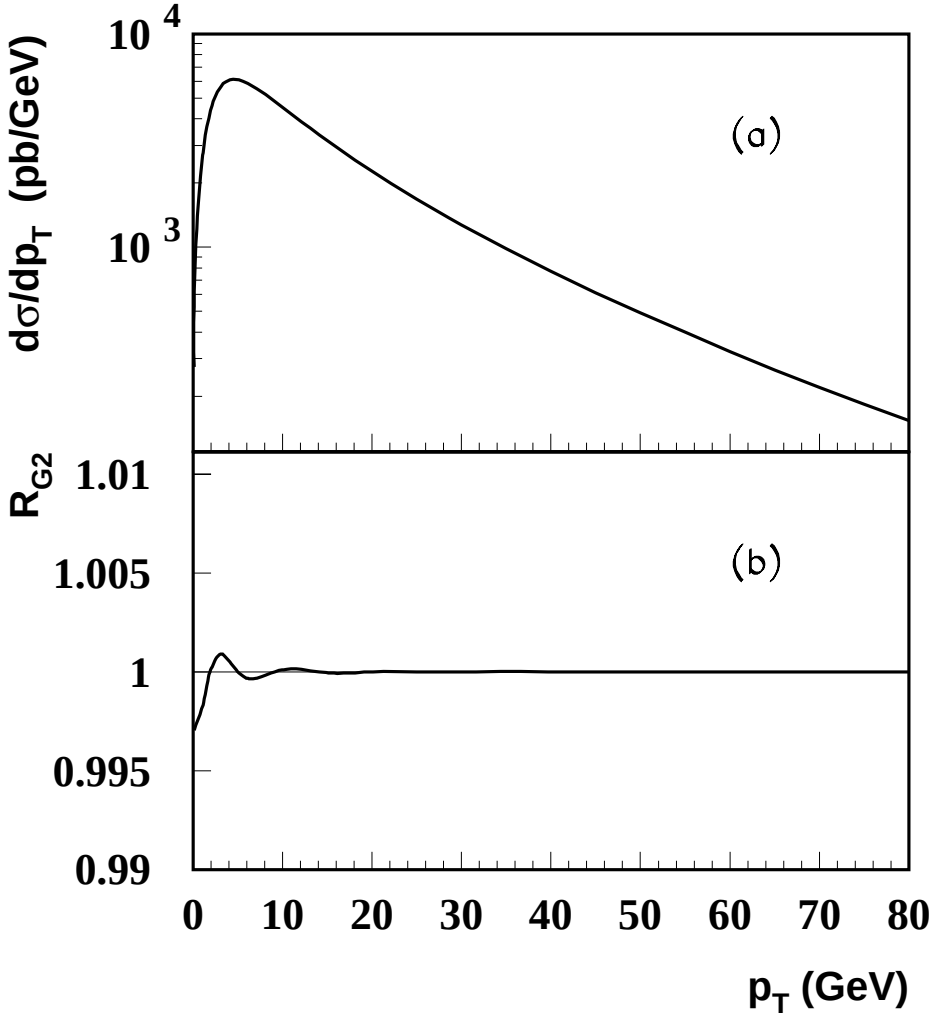

FIG. 7. (a) Cross section $\frac{d\sigma}{dp_T}$ for $W^{\pm}$ production in pp collisions at LHC with $\sqrt{s} = 14$ TeV; (b) R_{G_2} defined in Eq. (8) for $W^{\pm}$ at the same energy.

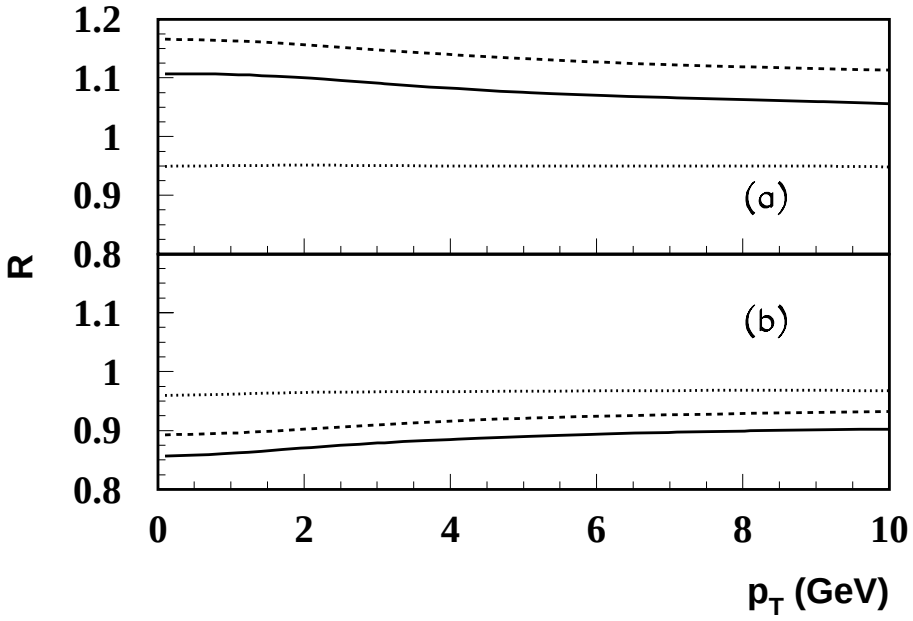

FIG. 8. (a) The isospin ratio, R_{iso}, defined in Eq. (9) (dashed line), the shadowing ratio, R_{sh}, defined in Eq. (10) (solid line), and "pure shadowing" (dotted) for Z^0 in $p + Au$ collisions at $\sqrt{s} = 350$ GeV; (b) same as (a) for $W^{\pm}$ production.

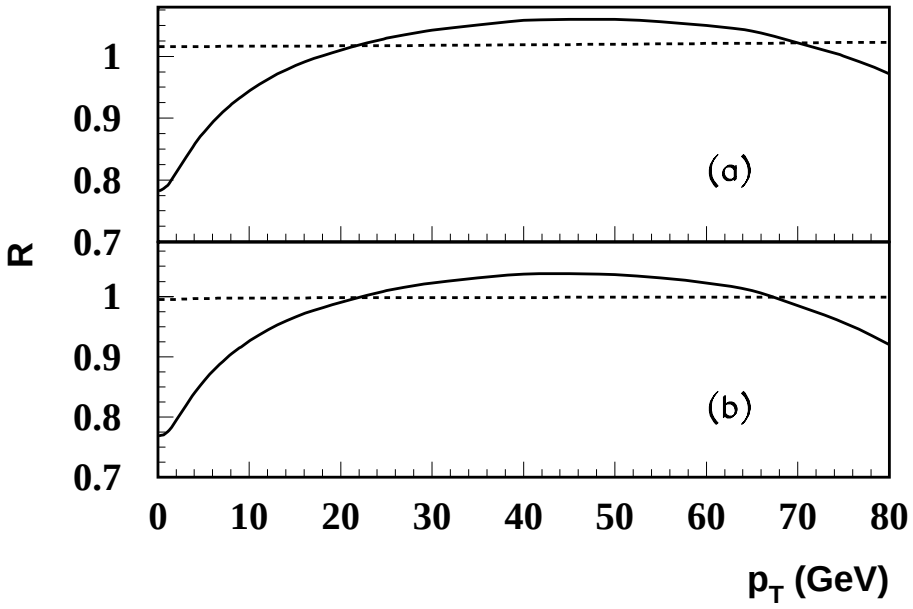

FIG. 9. (a) The isospin ratio, R_{iso} defined in Eq. (9) (dashed line) and the shadowing ratio, R_{sh}, defined in Eq. (10) (solid line) for Z^0 in $Pb + Pb$ collisions at $\sqrt{s} = 5.5$ TeV; (b) same as (a) for $W^{\pm}$ production.

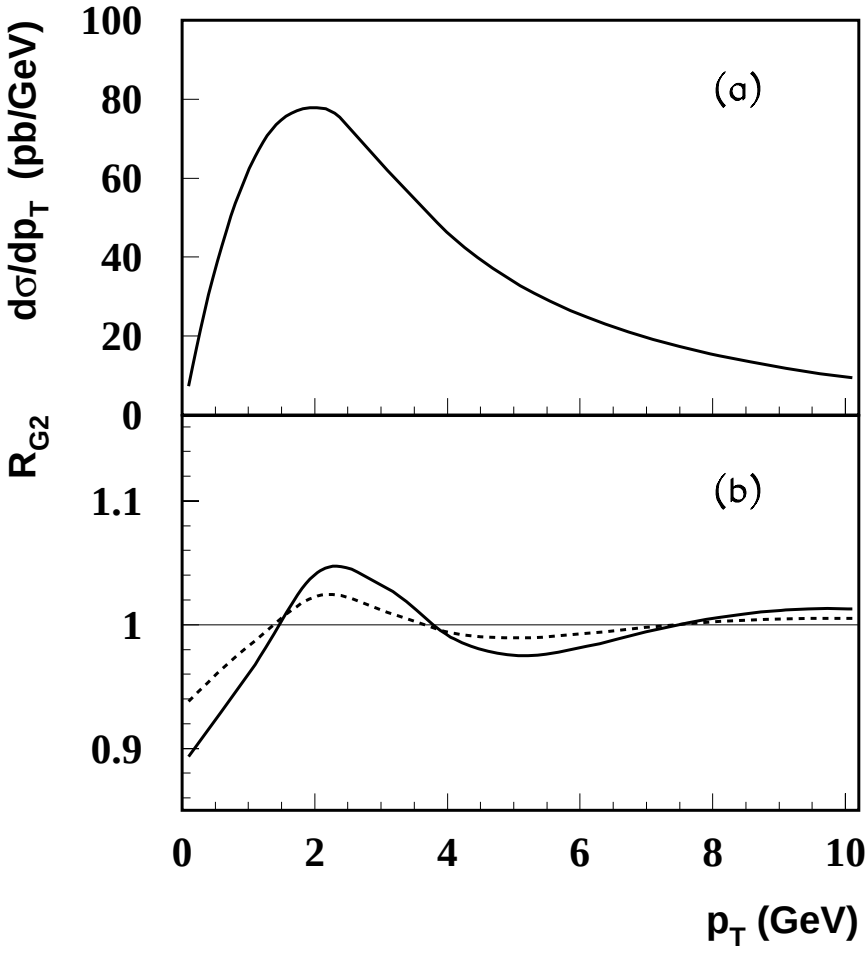

FIG. 10. (a) Cross section $\frac{d\sigma}{dp_T}^{(G_2,sh)}(p_T, Z_A/A, Z_B/B)$ for $W^{\pm}$ production in $p + Au$ collisions at RHIC with $\sqrt{s} = 350$ GeV averaged over AB; (b) The ratio $R^{sh}_{G_2}$ defined in Eq. (11) (solid line) in $p + Au$ collision and R_{G_2} defined in Eq. (8) for $W^{\pm}$ at the same energy.

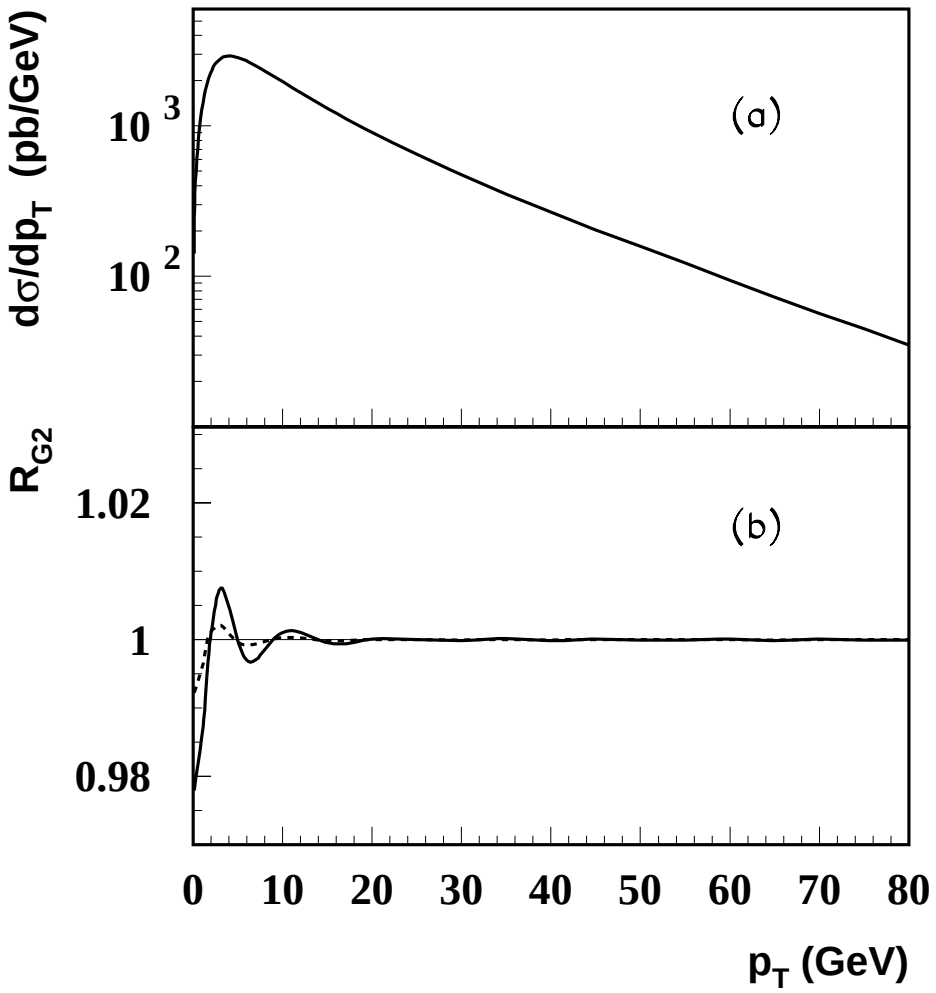

FIG. 11. (a) Cross section $\frac{d\sigma}{dp_T}^{(G_2,sh)}(p_T, Z_A/A, Z_B/B)$ for $W^{\pm}$ production in $Pb+Pb$ collisions at LHC with $\sqrt{s} = 5.5$ TeV, averaged over AB; (b) The ratio $R^{sh}_{G_2}$ defined in Eq. (11) (solid line) in $Pb + Pb$ collision and R_{G_2} defined in Eq. (8) for $W^{\pm}$ at the same energy.

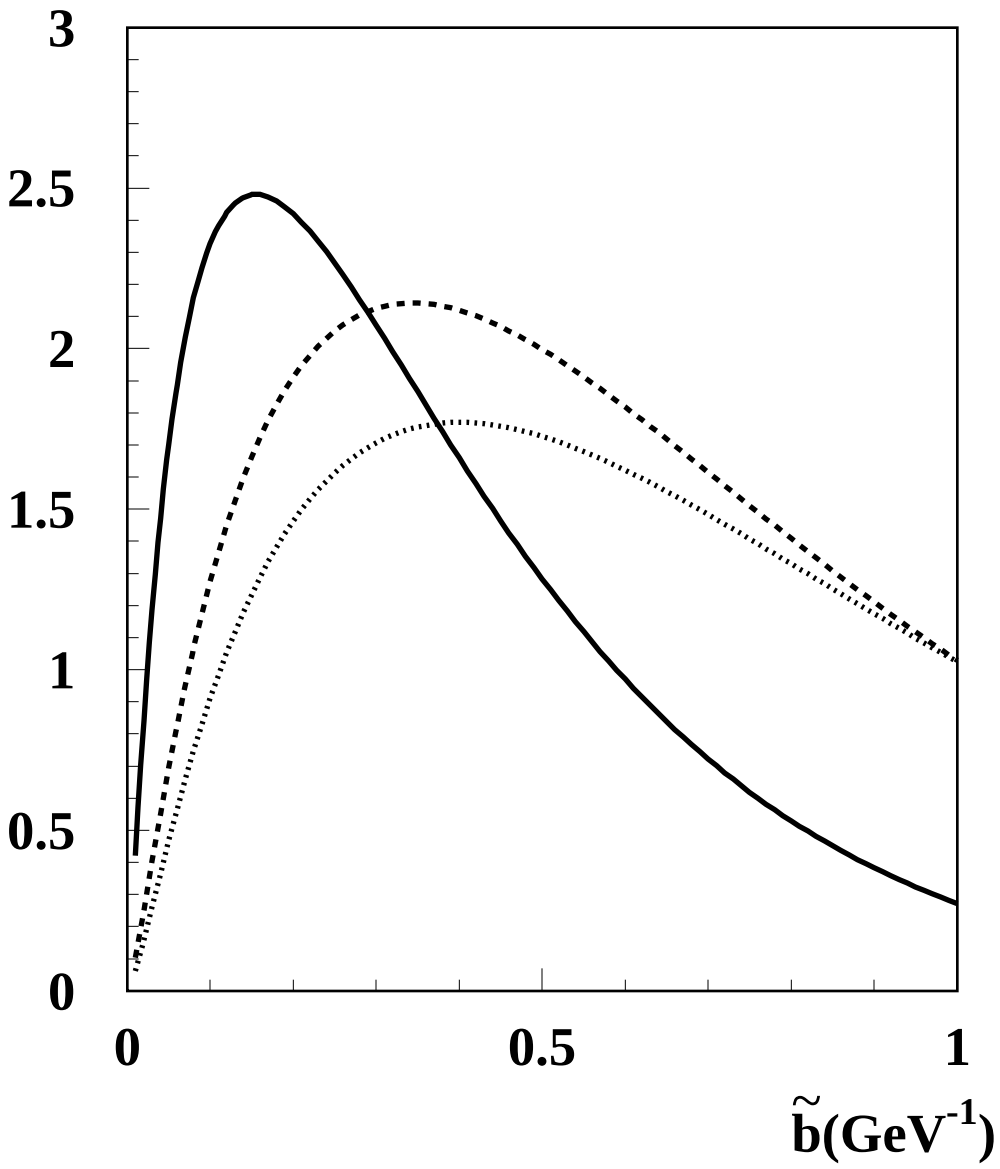
3
2.5
2
1.5
1
0.5
0
0
0.5
1
$\tilde{b}(GeV^{-1})$

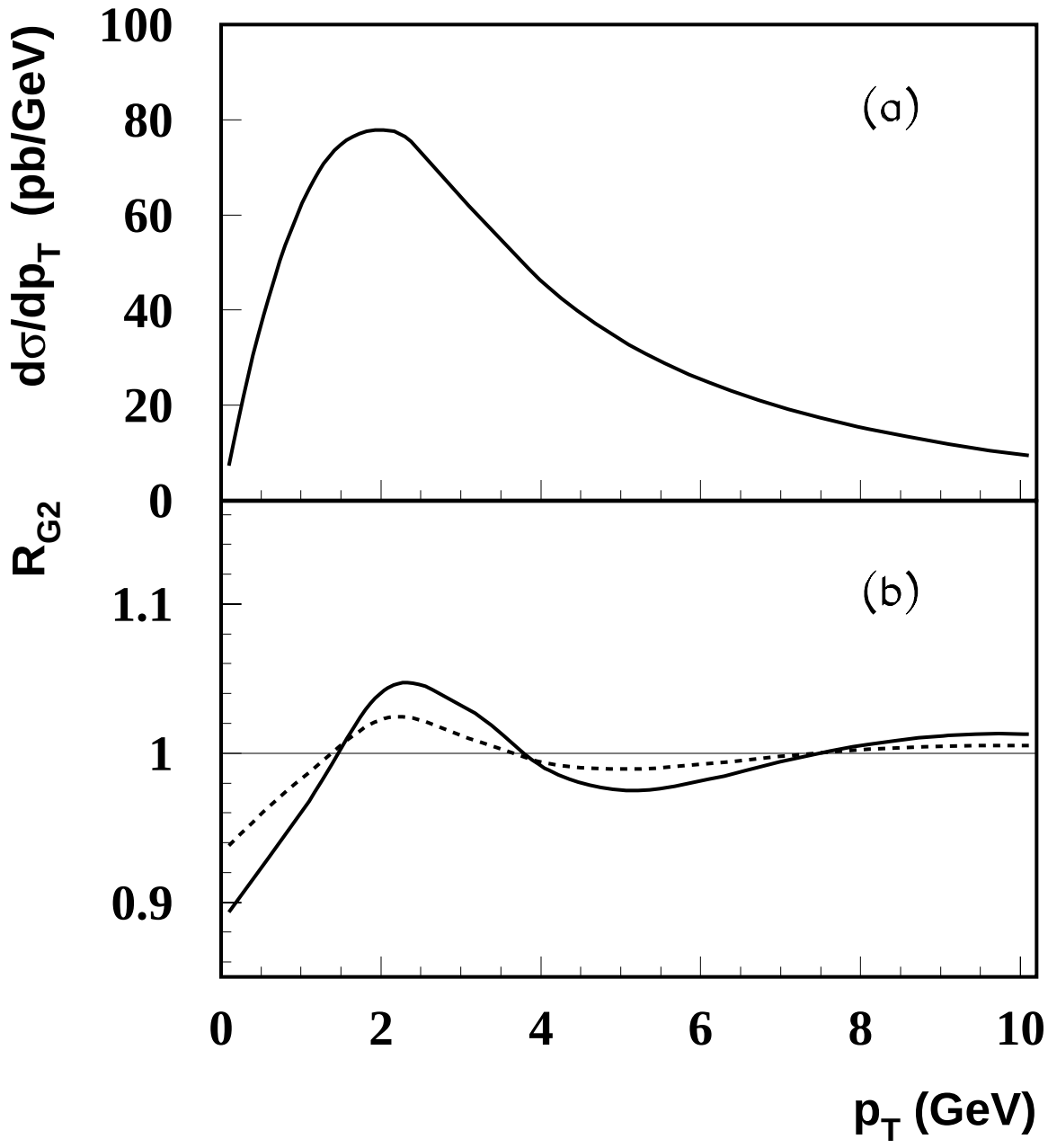
100
80
60
40
20
0
dσ/dp_T (pb/GeV)
(a)
R_G2
1.1
1
0.9
(b)
0
2
4
6
8
10
p_T (GeV)

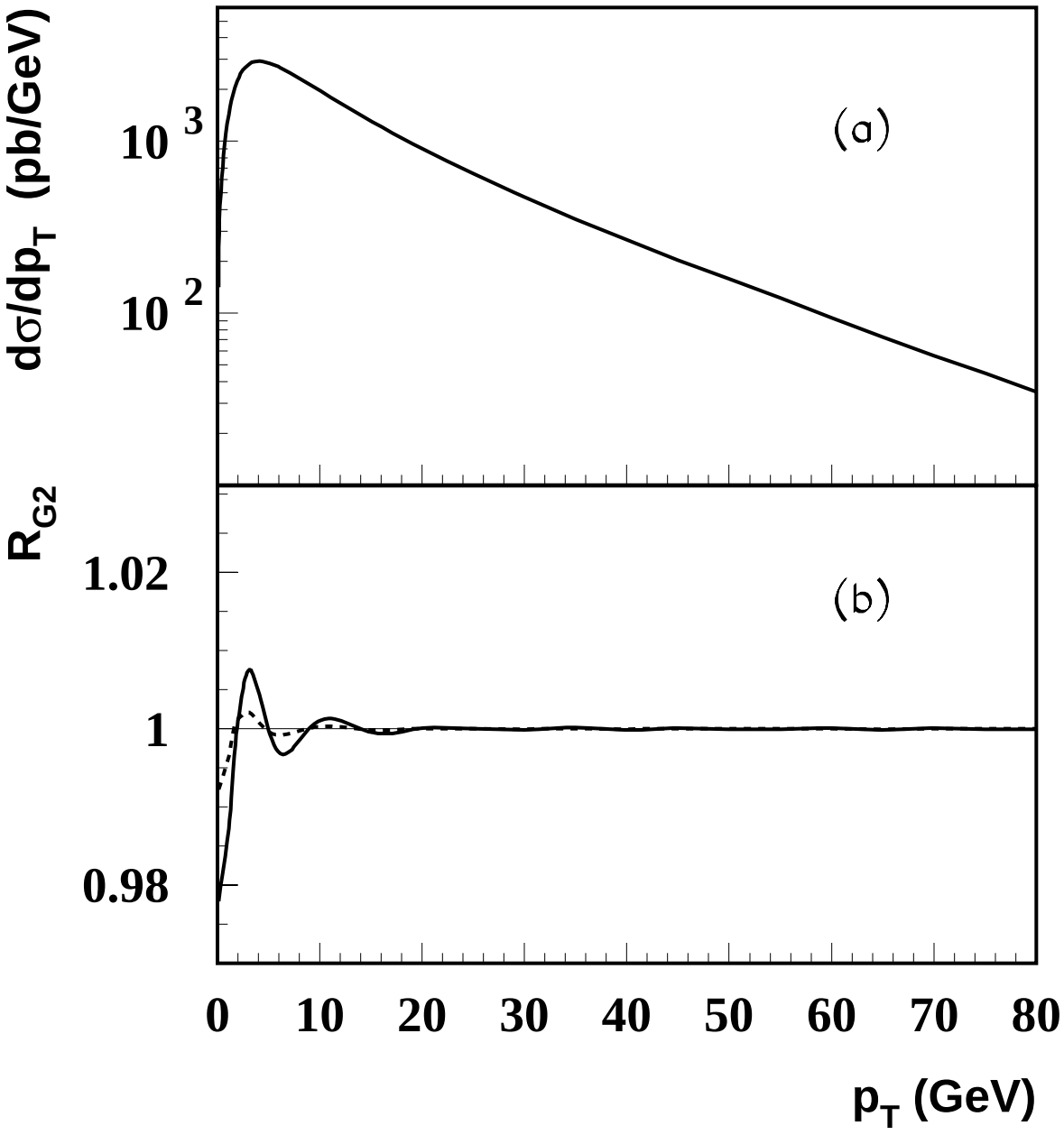
dσ/dp_T (pb/GeV)
10^3
10^2
(a)
R_G2
1.02
1
0.98
(b)
0
10
20
30
40
50
60
70
80
p_T (GeV)

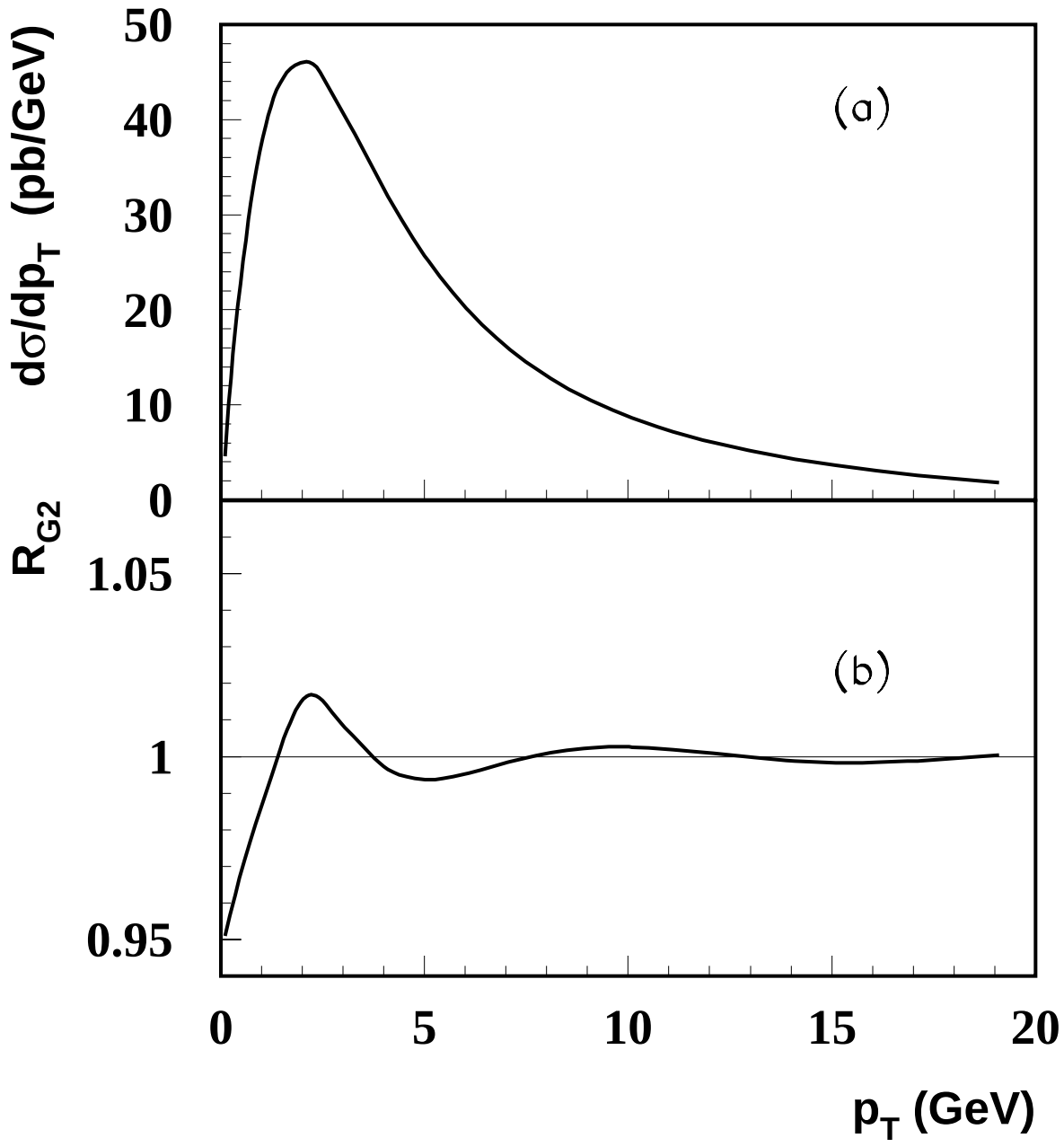
50
40
30
20
10
0
dσ/dp_T (pb/GeV)
(a)
R_G2
1.05
1
0.95
(b)
0
5
10
15
20
p_T (GeV)

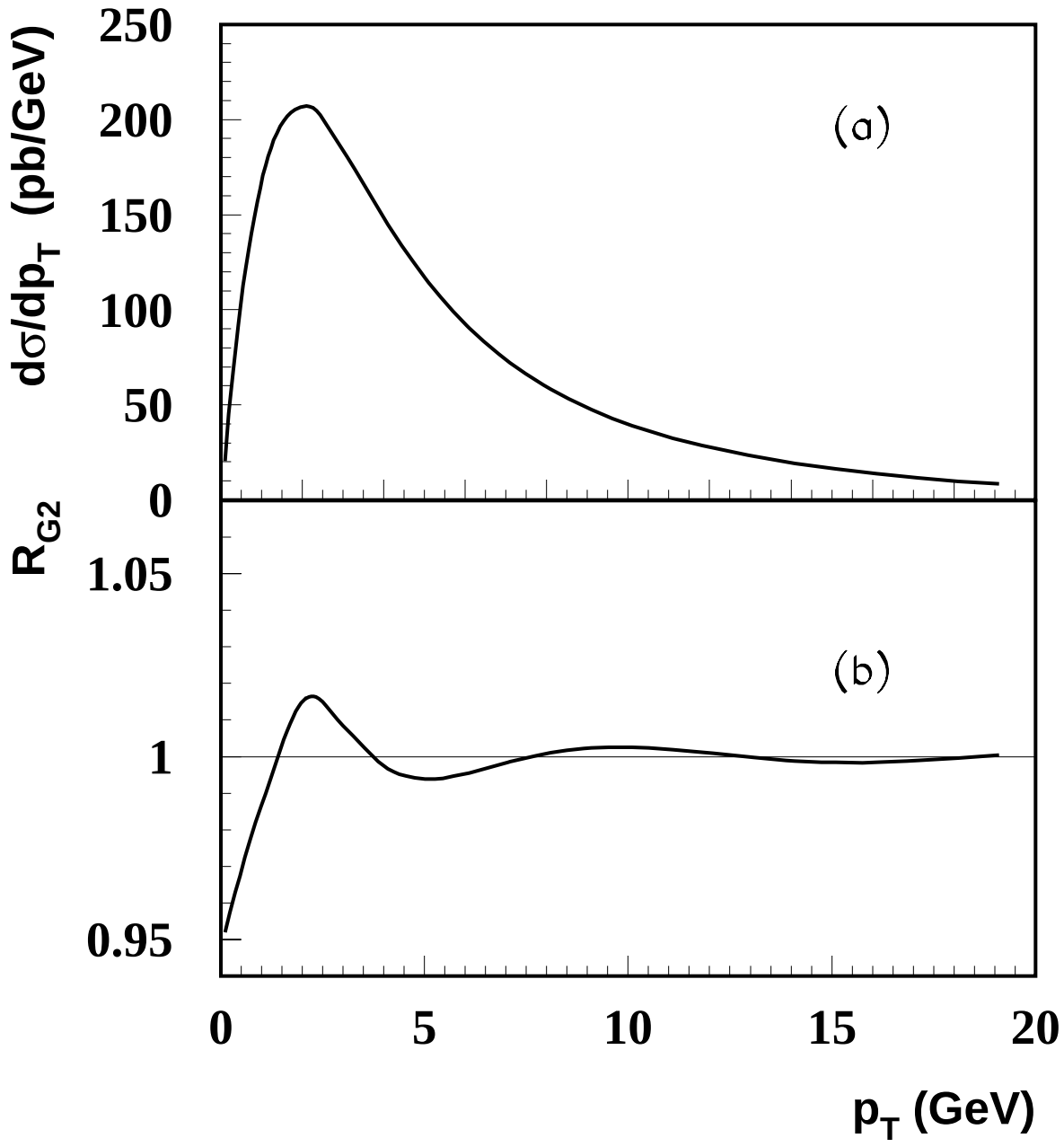
250
200
150
100
50
0
dσ/dp_T (pb/GeV)
(a)
R_G2
1.05
1
0.95
(b)
0
5
10
15
20
p_T (GeV)

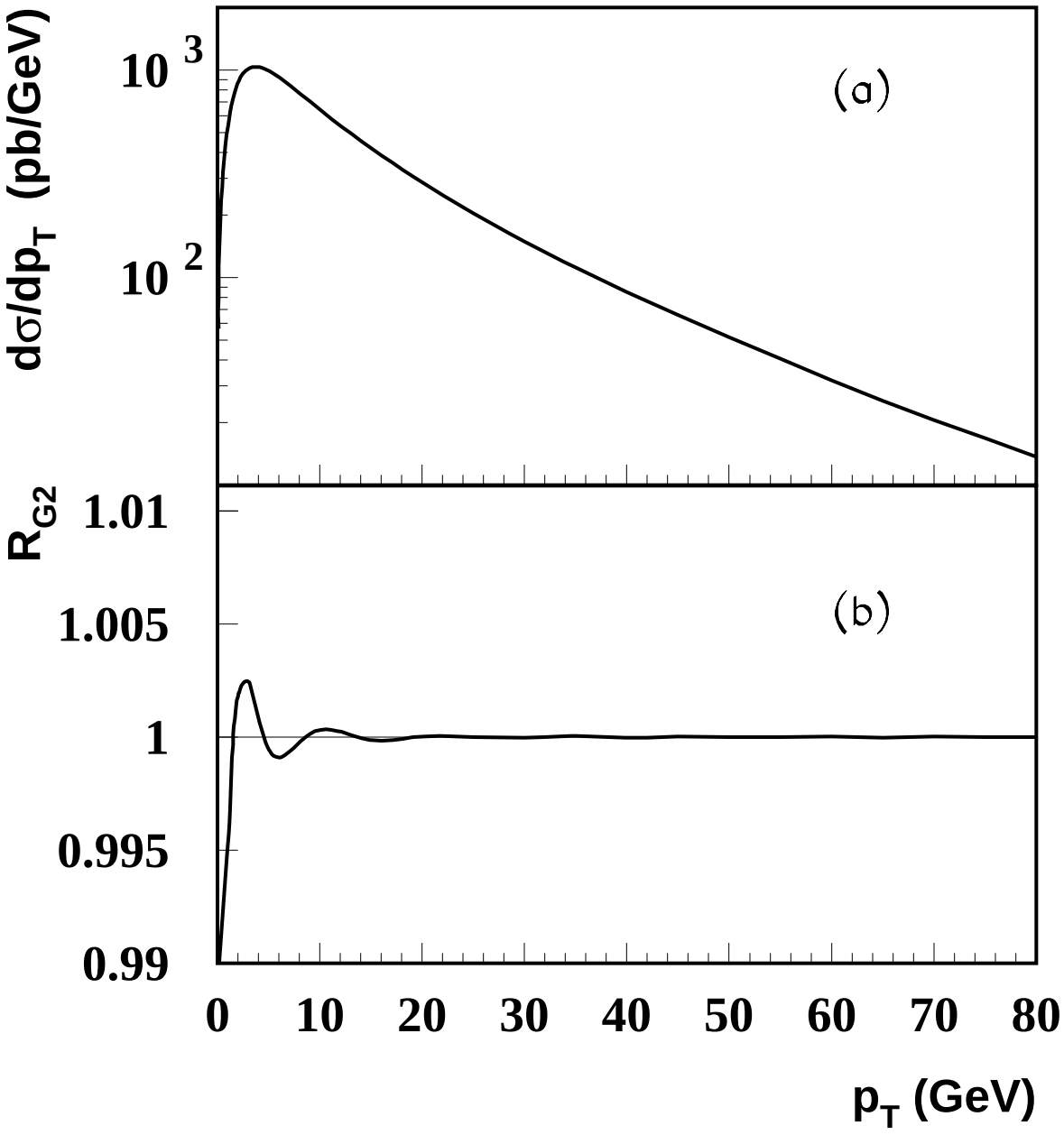
$d\sigma/dp_T$ (pb/GeV)
10^3
10^2
(a)
R_{G2}
1.01
1.005
1
0.995
0.99
(b)
0
10
20
30
40
50
60
70
80
p_T (GeV)

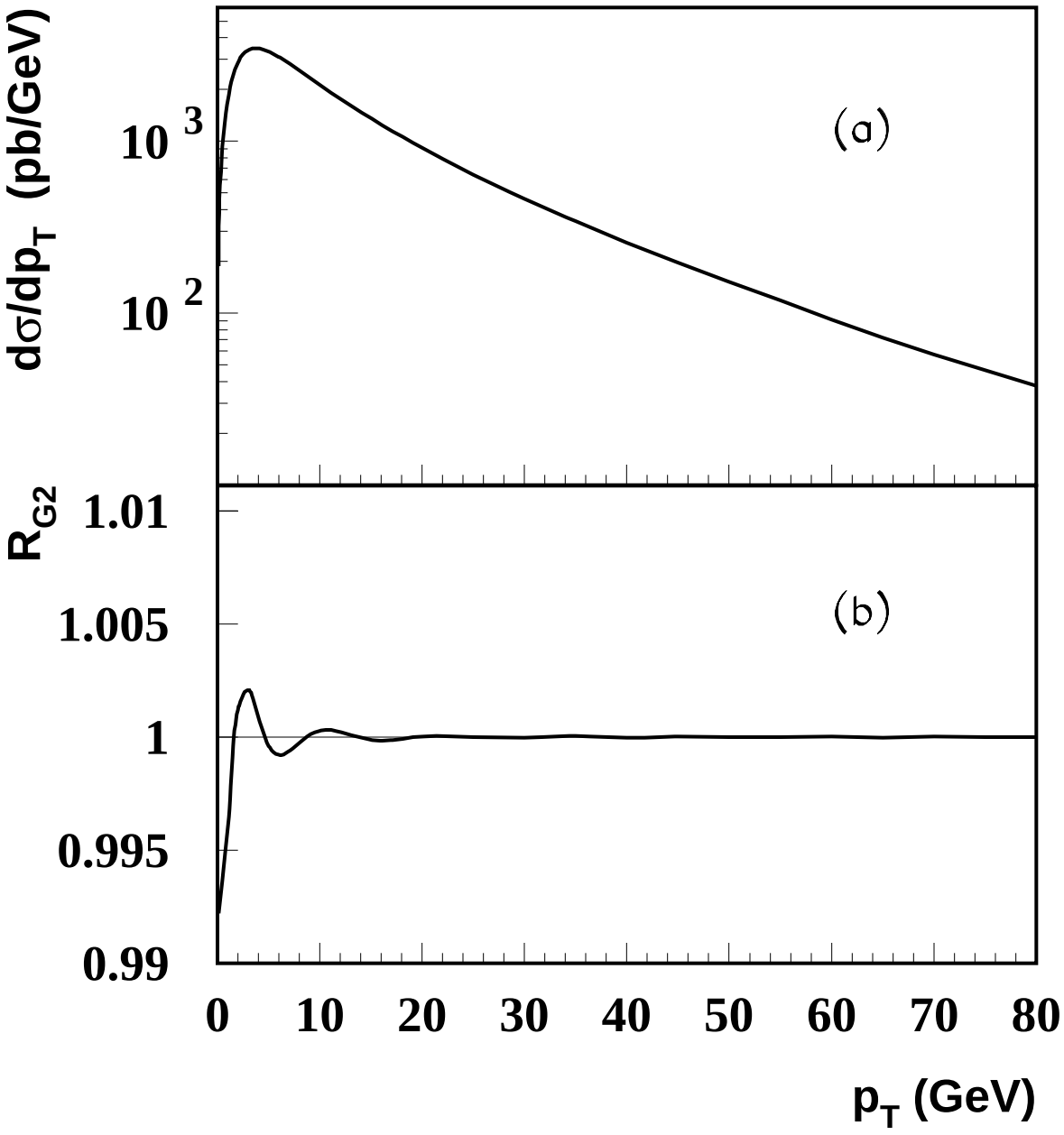
$d\sigma/dp_T$ (pb/GeV)
10^3
10^2
(a)
R_{G2}
1.01
1.005
1
0.995
0.99
(b)
0
10
20
30
40
50
60
70
80
p_T (GeV)

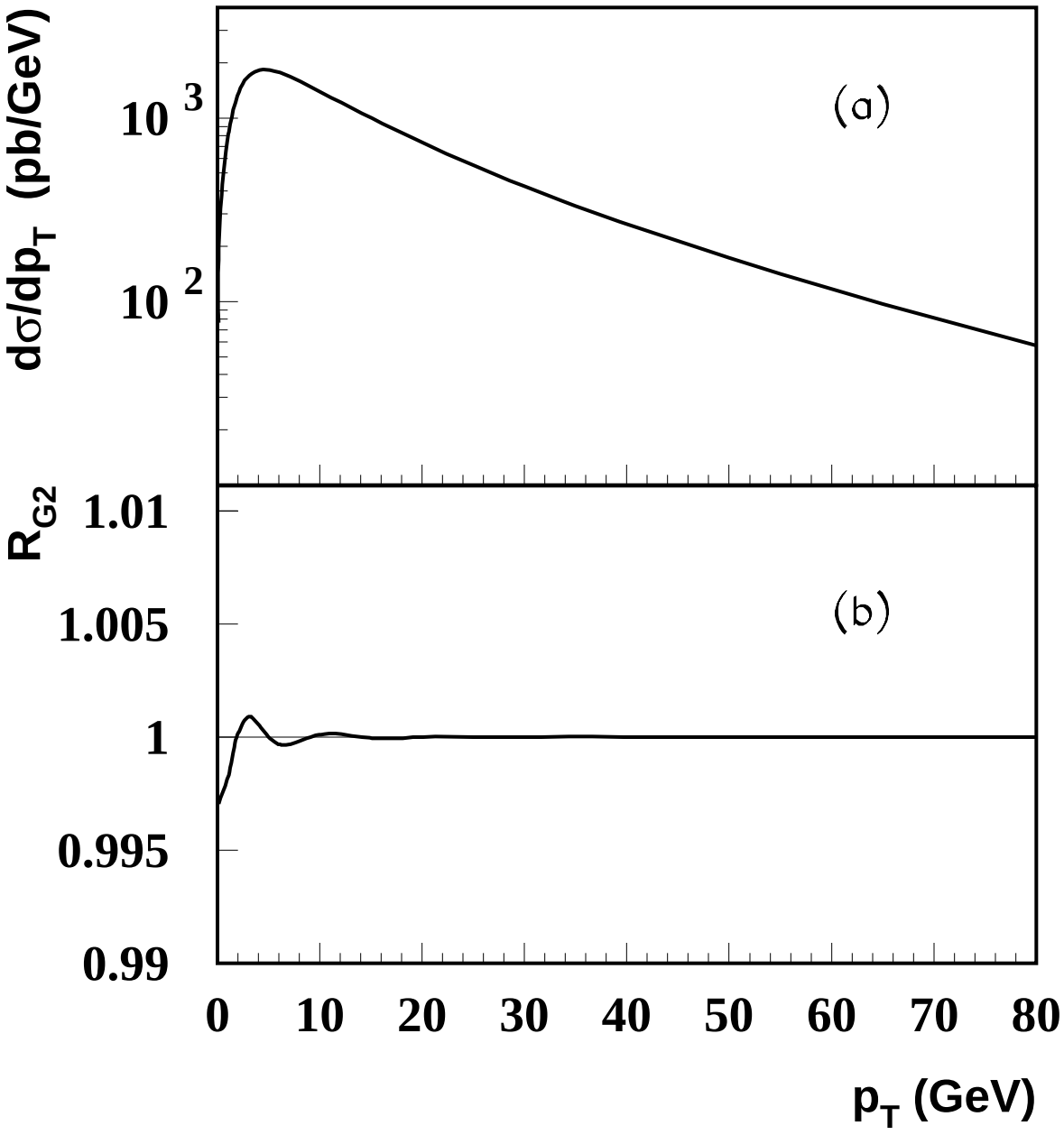
dσ/dp_T (pb/GeV)
10^3
10^2
(a)
R_G2
1.01
1.005
1
0.995
0.99
(b)
0
10
20
30
40
50
60
70
80
p_T (GeV)

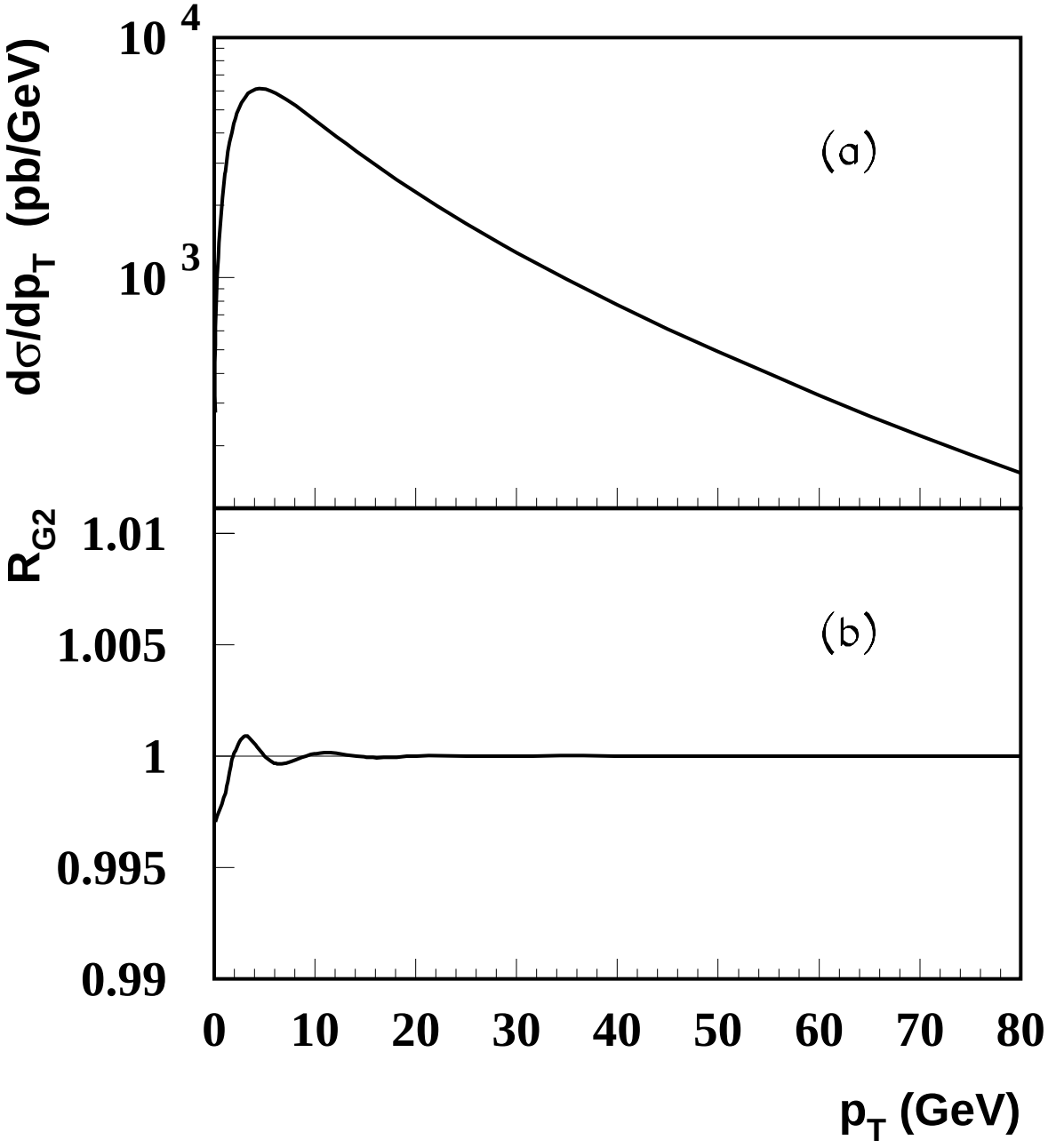
10^4
10^3
$d\sigma/dp_T$ (pb/GeV)
(a)
R_{G2}
1.01
1.005
1
0.995
0.99
(b)
0
10
20
30
40
50
60
70
80
p_T (GeV)

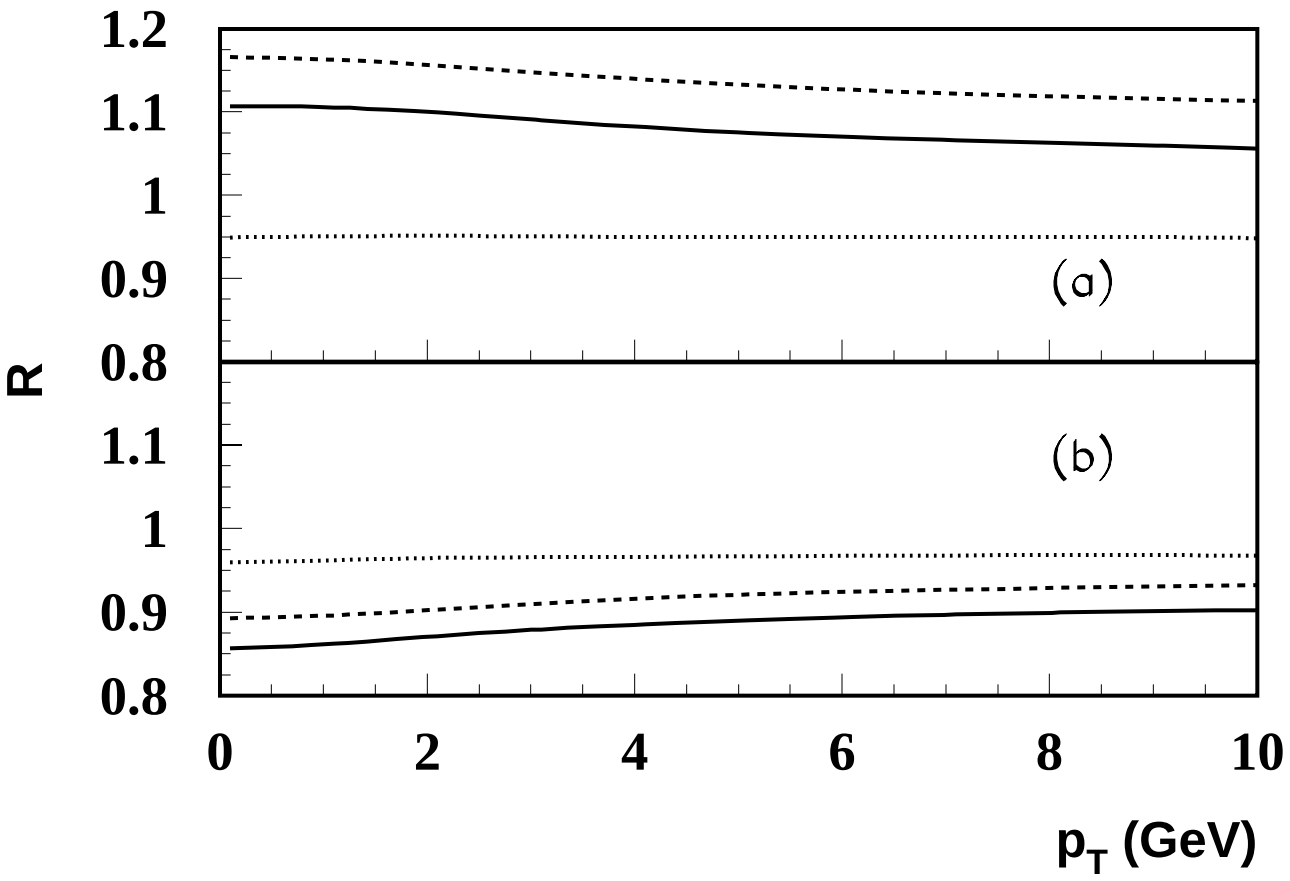
1.2
1.1
1
0.9
0.8
R
(a)
1.1
1
0.9
0.8
(b)
0
2
4
6
8
10
p_T (GeV)

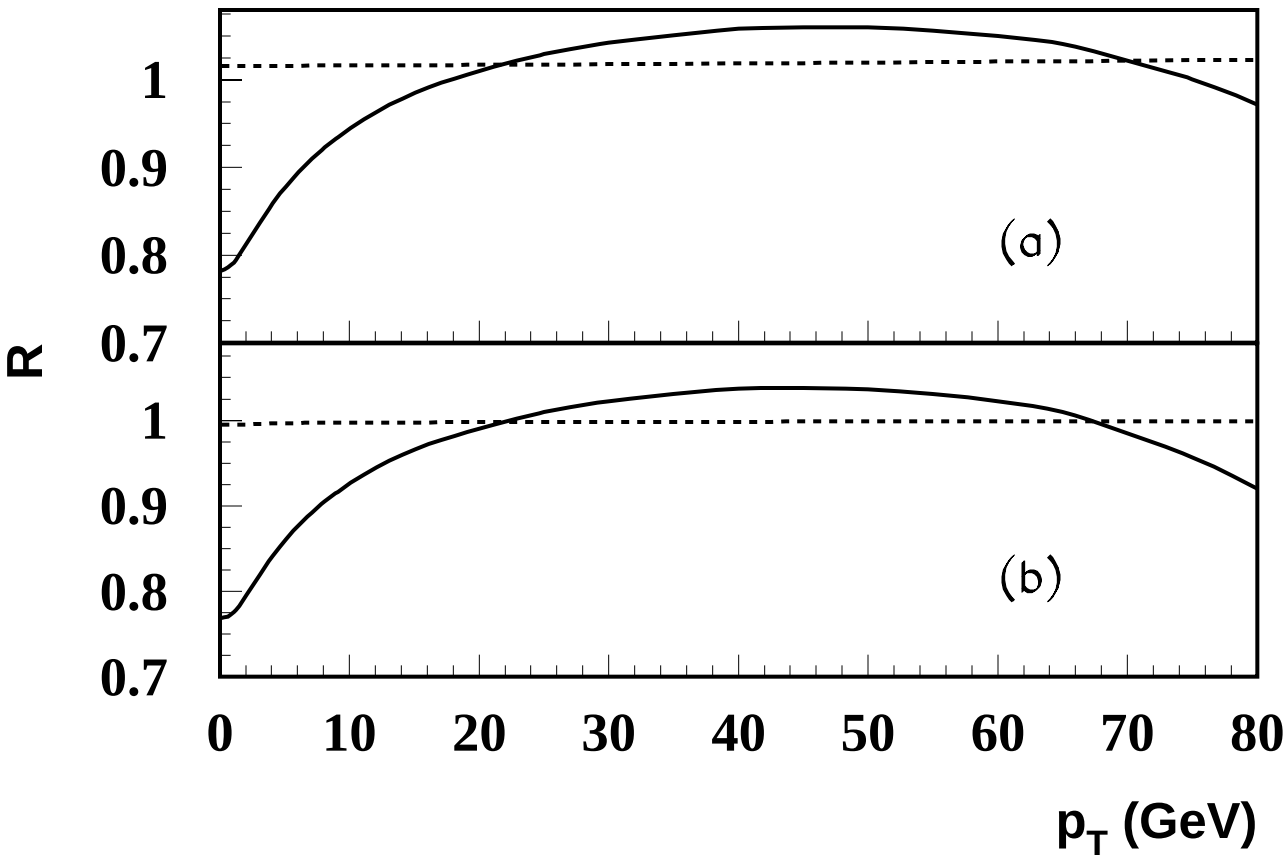
R
1
0.9
0.8
0.7
(a)
1
0.9
0.8
0.7
(b)
0
10
20
30
40
50
60
70
80
p_T (GeV)